

Thin Film Growth of $\text{Cu}(\text{In},\text{Ga})\text{S}_2$ by Reactive Annealing

The possibility of engineering the band gap of a $\text{Cu}(\text{In}_{1-x}\text{Ga}_x)\text{S}_2$ layer by simply adjusting the Ga-concentration at the interface and in the bulk of the layer offers great opportunities to tailor the band gap to the specific requirements of an electronic device. Therefore the precise control of the elemental composition, particularly of the $[\text{Ga}]/([\text{In}] + [\text{Ga}])$ ratio x of a $\text{Cu}(\text{In}_{1-x}\text{Ga}_x)\text{S}_2$ absorber layer is a prerequisite in order to fully utilize the potential benefits of Ga-alloying in $\text{Cu}(\text{In}_{1-x}\text{Ga}_x)\text{S}_2/\text{CdS}/\text{ZnO}$ heterostructures. This includes the fundamental understanding of the reactive and kinematic processes which govern the growth of the thin film. Such understanding eventually forms the basis for deliberately influencing the film formation process towards a desired Ga concentration or band gap profile respectively.

Therefore the thin film growth of Ga-free and Ga-containing $\text{Cu}(\text{In}_{1-x}\text{Ga}_x)\text{S}_2$ absorber layers by reactive annealing of Cu-In and Cu-(In,Ga) precursor stacks in rapid thermal processing (RTP) furnaces has been studied.

As will be shown below the sequential growth process can roughly be divided into three stages:

- 1.- precursor alloying,
- 2.- reactive annealing - incorporation of sulfur,
- 3.- reactive annealing - recrystallization.

The two step process used for absorber preparation was already outlined in Section 2.1. Interdiffusion and alloying of the metal layers in the precursor stack takes place during precursor deposition and precursor storage and in particular during substrate heat up of the reactive annealing step. As was shown by Wolf et al. [94] the kinetics of the reactive annealing step and the phase formation sequence depend on the initial state of the precursor. Whereas the phase composition and reaction kinetics of Cu-In and Cu-Ga bilayers are well documented in literature little data is available about the phase behavior of Cu-In-Ga multi stacks. In particular no report could be found about the time scale of intermetallic compound formation in such multilayers. Therefore, Section 3.1 compares the precursor phase composition of Cu-In bilayers and Cu-(In,Ga) triple layers as a function of deposi-

tion temperature and storage time.

Ex-situ monitoring has been applied to study the phase formation sequence during reactive annealing of the metal stacks in a sulfur containing atmosphere focusing on the influence of Ga-addition onto the formation of intermediate compounds and onto the reaction rate of the sulfurization process. Section 3.2 discusses the incorporation of the chalcogen into the metal precursor stack in terms of a diffusion controlled phase formation process. On the basis of the presented experimental results the sequential segregation of CuGaS_2 prior to CuInS_2 is identified as the decisive factor which is responsible for an inhomogeneous Ga-depth profile which is generally found in sequentially prepared $\text{Cu}(\text{In,Ga})\text{X}_2$ ($\text{X}=\text{S,Se}$) absorber layers [95].

As will be shown in Section 3.3 the final crystal quality of the absorber layer is only reached after the film undergoes a recrystallization process which immediately follows the incorporation of sulfur. The crucial role of the binary copper chalcogenide phase for the recrystallization process to become effective has been reported by numerous experiments [38, 96]. A tentative explanation of this recrystallization process will be proposed in Section 3.3.3. In case of Ga-containing absorber layers the copper-sulfide induced recrystallization process does not only lead to a structural improvement of the layer but also affects the Ga-depth profile as it is accompanied by an In-Ga interdiffusion process.

The discussed experimental results are summed up in a growth model in Section 3.4.

As mentioned above a precise knowledge of the Ga-concentration is crucial in order to deliberately influence the electronic properties of a heterojunction solar cell. Therefore Section 3.5 discusses the In-Ga interdiffusion process during the recrystallization stage of the film growth process which mainly determines the final Ga-depth profile of the absorber layer. As will be shown the Ga-concentration in the near surface region of the absorber layer, the region which mostly influences the photovoltaic parameters of the corresponding solar cell, is governed by a grain boundary diffusion process of Ga into the CuInS_2 thin films. A quantitative description of the diffusion process is given on the basis of numerical simulations.

3.1 Precursor Alloying

Cu-In and Cu-In-Ga metal stacks, deposited by physical vapor deposition (PVD), represent the starting point of the thin film growth process. The reaction kinetics and phase formation sequence depend on one hand on the initial stage of the precursor [94] and on phase transitions the precursor undergoes during substrate heat up of the reactive annealing step, but also on the other hand on the specific deposition technique [94, 97]. Hereby the phase composition and morphology of the precursor depend on the elemental composition of the layer, on the substrate temperature during precursor deposition, and, as will be shown in this section, on the sample storage time between precursor deposition and reactive annealing.

Cu is not soluble in In up to 430 K (Figure 3.1). It is interesting to note that Cu-rich phases known from bulk crystals do not form at thin film interfaces at room temperature even if the overall sample composition is Cu-rich [102].

In the Cu-In system the CuIn₂ phase decomposes above 150 °C into Cu-rich binary phases

Table 3.1: Chemical diffusion coefficient $D(T) = D_0 \exp(-E_a/k_B T)$ of Cu in In and Cu in Ga around room temperature.

Ref.	Cu→In Keppner et al. [100]	Cu→Ga Tikhomirova et al. [105]
D_0	$1.0 \times 10^{-6} \text{ cm}^2\text{s}^{-1}$	$1.34 \times 10^{-2} \text{ cm}^2\text{s}^{-1}$
E_a	0.42 eV	0.11 eV
T	300 K–340 K	300 K–430 K
$D(300 \text{ K})$	$8.8 \times 10^{-14} \text{ cm}^2\text{s}^{-1}$	$1.9 \times 10^{-4} \text{ cm}^2\text{s}^{-1}$

and liquid In [102]. The phase composition of Cu-In thin films at elevated temperatures agrees with the corresponding point in the phase diagram determined by the overall composition of the film. Whereas at room temperature the intermetallic compound formation was governed by Cu diffusion into the In layer at temperatures above $T = 150 \text{ °C}$ grain boundary diffusion of In into the Cu layer is the dominant transport mechanism [102]. In the Cu-Ga system the CuGa₂ phase is stable up to $\approx 250 \text{ °C}$. At higher temperatures phase formation at Cu-Ga interfaces proceeds in a similar way as in the Cu-In system [105], i.e. Ga diffuses into Cu and all intermetallic phases are Cu-rich.

Little work has been published about thin films consisting of Cu, In, and Ga. Hartmann [106] and Marudachalam et al. [95] have observed the effect of the addition of Ga onto the phase composition of sputtered Cu-In bilayers. Villora [107] has investigated thermally evaporated Cu-In and Cu-In-Ga stacks similar to the ones used in this work. No evidence for the existence of ternary Cu-In-Ga phases was reported by these authors. When comparing the experimental results of these works it can be concluded that the major difference of the phase composition with respect to the bilayer systems is the occurrence of unreacted In independently of sample composition or deposition temperature. However, the time scale at which the observed intermetallic phase transitions occur has not been discussed.

3.1.2 Precursor Phase Composition

Bilayers Cu-In and Cu-Ga stacks have been PVD deposited at room temperature and the phase composition has been observed by X-ray diffraction as a function of storage time. A similar set of samples was deposited at 300 °C. All bilayers were Cu-rich, i.e. $[\text{Cu}]/([\text{In}]+[\text{Ga}]) > 1.0$.

Right after deposition of In (300 nm) onto a Cu film (atomic ratio $[\text{Cu}]/[\text{In}] = 1.7$) metallic

In and Cu are the only phases in the stack. XRD-spectra repeatedly taken during the first 24 hours after deposition show that on a time scale of a few hours CuIn_2 forms on the expense of free In (Figure 3.2 (a)). Ten hours after deposition the entire 300 nm thick

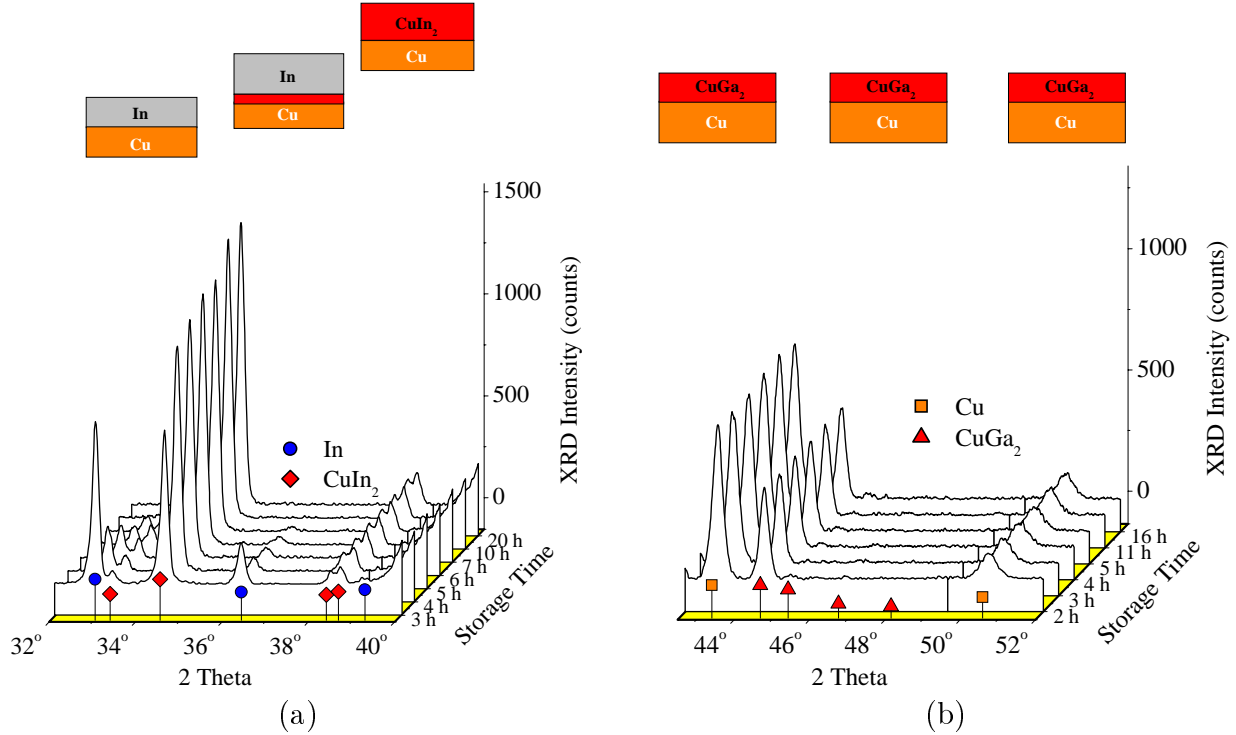


Figure 3.2: Sections of XRD spectra of (a) a Cu-In bilayer (Cu = 400 nm, In = 300 nm) and (b) a Cu-Ga bilayer (Cu = 400 nm, Ga = 160 nm) measured after different storage intervals.

In layer has reacted to CuIn_2 and the phase composition, i.e. Cu and CuIn_2 , remains unchanged for several weeks. This is in reasonable agreement with the Cu-In chemical diffusion coefficient D given Table 3.1, which predicts a layer thickness of $d = \sqrt{Dt} \approx 500$ nm after 10 h. Cu-In bilayer composition is shifted to more Cu-rich binary phases when the metal layers are deposited at 300 °C, where CuIn_2 is not stable anymore. Depending on the overall Cu-excess in the stack $\text{Cu}_{11}\text{In}_9$ and/or $\text{Cu}_{16}\text{In}_9$ (η' modification [103]) can be found. No changes in phase composition with storage time could be observed. A Cu-Ga stack ($[\text{Cu}]/[\text{Ga}] = 4$) deposited at room temperature mainly consists of metallic Cu and CuGa_2 (Figure 3.2 (b)). However, in contrast to the Cu-In stack, alloying already takes place during or immediately after deposition due to rapid diffusion of Cu into the Ga-layer. There is no increase in CuGa_2 XRD-peak intensity with storage time nor any reflections that could be assigned to metallic Ga. Similarly to the Cu-In bilayers no Cu-rich binary phases were found, which indicates the absence of any Ga-diffusion into the Cu-layer. In view of the equilibrium phase diagram which predicts a wide region of Ga-solubility in Cu (α -phase in Figure 3.1) this is rather surprising and indicates a strong kinetic limitation for the diffusion process.

At a deposition temperature of 300 °C Cu-Ga bilayers consist of Cu_9Ga_4 and metallic Cu.

Similarly to CuIn₂ the CuGa₂ phase is not stable at this temperature.

Triple-layers The addition of Ga to the metal stack was realized by evaporating a Ga-layer onto a just evaporated Cu-In bilayer. Since In and Ga are soluble over the entire composition range [99] the still unreacted In of the Cu-In bilayer will intermix with the evaporated Ga, hence in the following triple layers will be referred to as Cu-(In,Ga) samples. Figure 3.3 shows sections of XRD spectra of such a Cu-(In,Ga) sample ($[\text{Cu}]/([\text{In}] + [\text{Ga}]) = 1.7$, $[\text{Ga}]/([\text{In}] + [\text{Ga}]) = 0.3$) deposited at room temperature. After deposition Cu, CuGa₂ and free In are the most prominent phases in the thin film sample. After several days of storage CuIn₂ reflexes can be found in addition (Figure 3.3 (a)). However, in comparison to the bilayer samples CuGa₂ and in particular CuIn₂ formation proceeds much slower. Even four weeks after deposition unreacted Cu and In are still present in the layer.

The reduced reaction rate in Cu-(In,Ga) samples is also evident in thin films deposited at elevated temperatures. When depositing at 300 °C some of the In has alloyed to Cu₁₁In₉ and/or Cu₁₆In₉ whereas Cu and Ga forms Cu₉Ga₄, however even after a deposition at 300 °C there is still unreacted In in the layer.

There is a slight but systematic shift in the peak position of the XRD reflection of the CuGa₂ binary phase to lower diffraction angles, which can be assigned to a widening of the unit cell caused by a partial replacement of Ga atoms by larger In atom. In a similar way the XRD-reflections of the Cu₁₆In₉ in triple layer samples deposited at 300 °C are shifted to higher angles which indicates the partial incorporation of Ga into this phase.

Table 3.2 summarizes the observed reaction times for intermetallic phase formation in the bilayer and triple-layer samples at room temperature. Thicknesses of the binary compounds were estimated using values for the mass density as given by [99, 100]. The last four columns of the table compare the observed times t required for complete layer formation to calculated reaction times τ based on the diffusion coefficients given in Table 3.1.

Table 3.2: Reactions times for thin film intermetallic compound formation at room temperature. (t = observed time, τ = estimated time)

stacking sequence	d_{In}	d_{Ga}	d_{CuIn_2}	d_{CuGa_2}	t_{CuIn_2}	t_{CuGa_2}	τ_{CuIn_2}	τ_{CuGa_2}
Cu-In	300 nm		315 nm		10 h		3.1 h	
Cu-Ga		160 nm		190 nm		< 0.5 h		< 1 s
Cu-(In,Ga)	400 nm	70 nm	420 nm	83 nm	>1600 h	< 0.5 h		

In the room temperature triple layer samples the presence of free Cu and free In on one hand and CuGa₂ on the other hand verifies the higher reaction rate of CuGa₂ formation compared to CuIn₂ formation, as observed in the bilayer samples. However, in Cu-In bilayers all In alloys after some hours, whereas in Cu-(In,Ga) layers free In can be found even after weeks of storage, which indicates a kinetic limitation for the formation of Cu-In

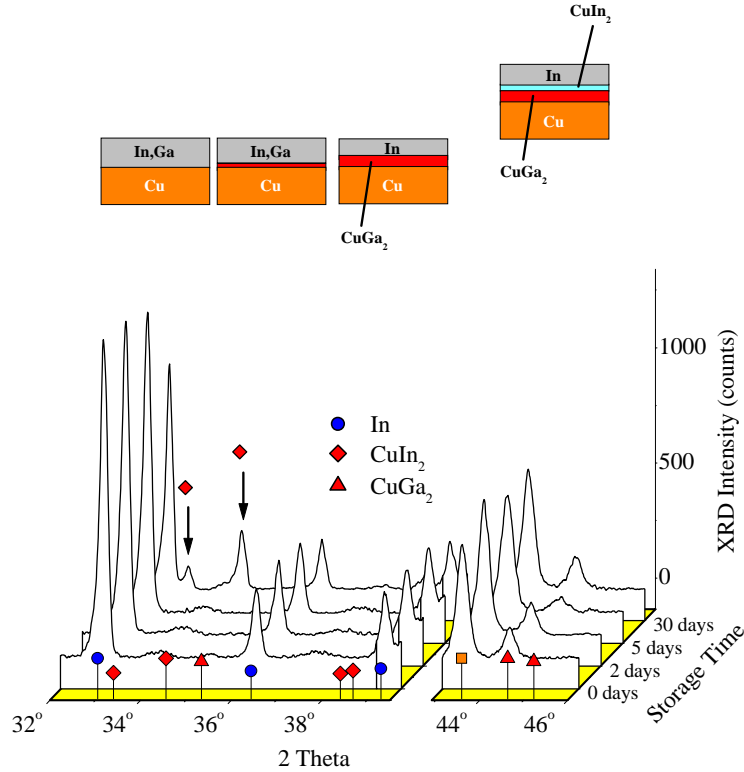


Figure 3.3: Sections of XRD spectra of Cu-(In,Ga) triple-layer deposited at room temperature measured after different storage intervals (initial stacking sequence: Cu = 600 nm, In = 420 nm, Ga = 70 nm).

alloys due to the presence of Ga. At 300 °C, where the metal diffusivities can be assumed to be much higher, the effect is less pronounced. Nevertheless unreacted In can also be found at these samples after deposition. In the case of the Ga-free samples there was no In anymore right after deposition at 300 °C. Thus, even at 300 °C the presence of Cu_9Ga_4 significantly delays Cu-In alloying.

Villora [108] tentatively suggested that solid CuGa_2 at the Cu-(In,Ga) interface, which, as shown above, forms much more rapidly than CuIn_2 , acts as an interdiffusion barrier leading to the observed strongly delayed formation of Cu-In alloys. This could be experimentally verified by depositing In thin films onto already alloyed Cu/ Cu_9Ga_4 bilayers. The phase formation of these samples remained unchanged for several months which clearly shows the the Cu_9Ga_4 phase in between the Cu and the In layer effectively blocks any Cu-In alloying.

The crucial role of a Cu-Ga binary phase at the Cu-(In,Ga) interface for Cu-In interdiffusion could also be confirmed by another experiment where a Cu-In-Cu-Ga multi stack was deposited at room temperature. In such a stack Cu-In and Cu-Ga interdiffusion should be spatially separated and indeed all In alloys to CuIn_2 in such a multi stack. This supports the assumption of an Ga-induced diffusion barrier at the Cu-In interfaces which suppresses

Cu-In intermixing at room temperature.

Finally, Table 3.3 gives an overview over the observed precursor phase formation depending on precursor stacking sequence, deposition temperature and storage time.

Table 3.3: Phases observed at Cu-In bilayers and Cu-In-Ga triple-layers deposited at room temperature (RT) and at 300 °C. Phases were determined by XRD.

stacking sequence	$\frac{[\text{Cu}]}{[\text{In}]+[\text{Ga}]}$	$\frac{[\text{Ga}]}{[\text{In}]+[\text{Ga}]}$	RT deposition	RT deposition two weeks storage	300 °C deposition
Cu-In	1.7		Cu, In	Cu, CuIn_2	Cu, $\text{Cu}_{11}\text{In}_9$, $\text{Cu}_{16}\text{In}_9$
Cu-Ga	2		Cu, CuGa_2	Cu, CuGa_2	Cu, Cu_9Ga_4
Cu-(In,Ga)	1.8	0.3	Cu, CuGa_2 , In	Cu, CuGa_2 , CuIn_2 , In	Cu_9Ga_4 , $\text{Cu}_{16}\text{In}_9$, In
(Cu,Ga)-In	1.8	0.3	Cu, Cu_9Ga_4 , In	Cu, Cu_9Ga_4 , In	
Cu-In-Cu-Ga	1.8	0.3	Cu, CuIn_2 , CuGa_2		$\text{Cu}_{11}\text{In}_9$, Cu_9Ga_4

In conclusion room temperature alloying in Cu-In and Cu-Ga bilayers is governed by Cu diffusion into In or Ga leading to Cu and CuIn_2 or CuGa_2 respectively. Cu-In alloying in typical precursor structures proceeds on a time scale of several hours whereas Cu-Ga alloying takes place during or immediately after bilayer deposition. Although overall sample composition was Cu-rich no Cu-rich binary phases could be observed at room temperature, which indicates a strong kinetic limitation for the diffusion of Ga or In into Cu. At 300 °C no kinetic limitations in intermetallic compound formation could be observed in bilayer samples and the phase composition of precursor deposited at 300 °C agrees with the equilibrium phase diagram. There are no further changes in phase composition with storage time.

Phase formation in Cu-In bilayers is strongly altered by the presence of Ga. It could be shown that a Cu-Ga binary phase at the Cu-(In,Ga) interface strongly suppresses Cu-In alloying, thereby leading to significant amounts of metallic In even after weeks of storage. The strong kinetic limitation for Cu-In alloying imposed by the presence of Ga can only partially be overcome when raising the substrate temperature during precursor deposition. However, it could be shown that the spatial separation of the In and Ga layer by an additional Cu layer avoids the occurrence of unalloyed In. The effects of unalloyed In in the Cu-(In,Ga) precursor layers, when transforming the metal stack to a chalcopyrite in a sulfur containing atmosphere, will be discussed in the next section.

3.2 Reactive Annealing - The Incorporation of Sulfur

This section investigates the transformation of the metallic precursor stacks into chalcopyrite thin films. Before presenting the experimental results the phase equilibria in the Cu-In-Ga-S will be briefly discussed by means of equilibrium phase diagrams and thermodynamical equilibrium calculations and compared to reports on the growth process of Ga-free CuInS_2 layers, where several publications can be found in literature [63, 64, 109, 110], and to published results on single crystal growth of $\text{Cu}(\text{In}_{1-x}\text{Ga}_x)\text{S}_2$ [27–30]. Then the experimentally observed phase formation sequence for reactive annealing of Ga-containing and Ga-free metallic precursors will be outlined. As will be shown the addition of Ga to the metallic precursor leads to the segregation of two $\text{Cu}(\text{In}_{1-x}\text{Ga}_x)\text{S}_2$ phases with composition $0 \leq x < 0.15$ and $0.75 < x \leq 1$ causing a highly inhomogeneous Ga-depth distribution. Furthermore, in the case of reactive annealing in sulfur vapor, the direct phase formation process of CuInS_2 directly from the metal phases is shifted to a more indirect growth path involving an intermediate CuIn_5S_8 phase. By means of depth resolved Raman spectroscopy measurements at partially processed layers the incorporation of sulfur into the metal film via a diffusion controlled process will be explained.

3.2.1 $\text{Cu}_2\text{S-In}_2\text{S}_3$ Phase Behavior

In order to understand the phase formation of ternary I-III-VI₂ compounds their phase equilibria can be discussed in terms of temperature and composition. The ternary compositional triangle has already been discussed in Section 1.1.2. A diagram of the $T - x$ relation along the $\text{Cu}_2\text{S-In}_2\text{S}_3$ pseudo-binary line is given in Figure 3.4. This section of the ternary field is characterized by $\Delta y = 0$, i.e. the valency requirements of a filled anion octet is fulfilled for all compositions. Whereas temperature induced changes at stoichiometric compositions lead to cation order-disorder effects or changes in the crystal structure, variations in composition cause the formation of secondary phases. Besides CuInS_2 there is only one more ternary equilibrium phase, i.e. CuIn_5S_8 , which has a spinel structure. As can be seen in Figure 3.4 the single phase chalcopyrite γ phase exists over an extended range of compositions, hence slight deviations from the ideal stoichiometry are compensated by the incorporation of lattice defects rather than secondary phase segregation. The width of the homogeneity region gets wider with increasing temperature. At temperatures below 500 °C the region is asymmetric and extends about 2 mole % towards In_2S_3 . On the other hand over-stoichiometric Cu concentrations will immediately result in the precipitation of the secondary Cu_2S phase. At high temperature the ternary chalcopyrite CuInS_2 phase undergoes two phase transitions. At 980 °C a cation order-disorder transition occurs which leads to the zincblende δ phase. At 1045 °C the δ phase transforms to a ζ phase, of still unknown structure (possible wurtzite) [111]. The existence of disorder prior to melting in chalcopyrite compounds has been discussed by several authors [111,112]. Binsma [111]

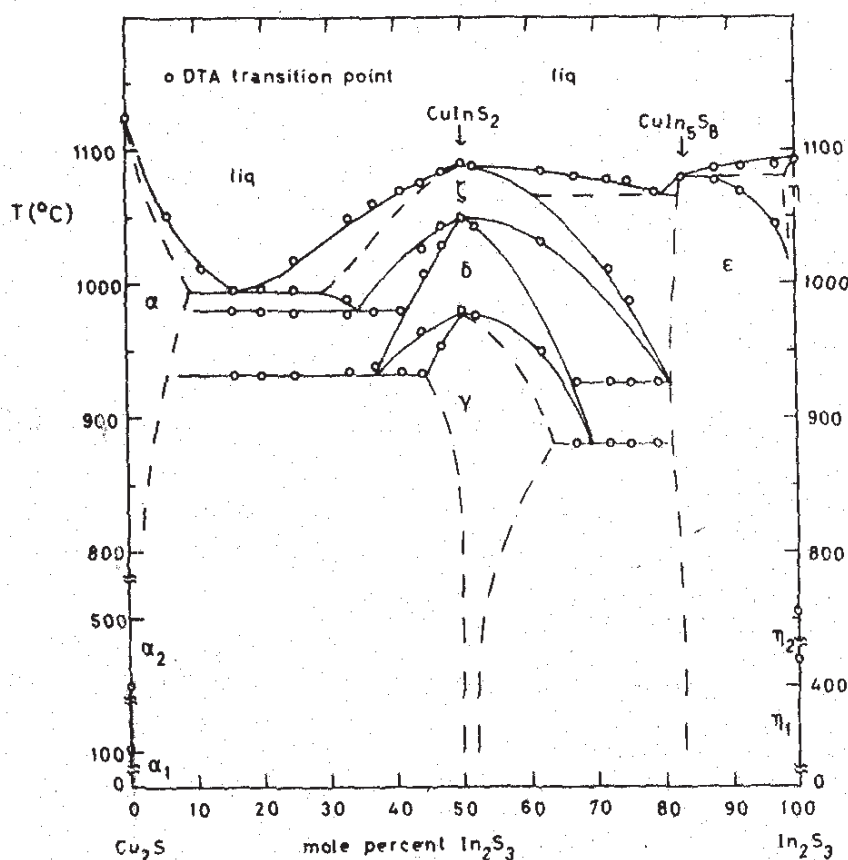


Figure 3.4: Pseudo-binary phase diagram of CuInS_2 Ref. [111].

has correlated the occurrence of an order-disorder transition to the tetragonal distortion of the chalcopyrite unit cell, where materials with $\eta = c/a > 1.95$ generally show such a transition. In the case of CuGaS_2 the c/a ratio, according to literature data of several authors [23, 24], lies in the range of 1.948–1.963, however a disorder transition has not been observed so far.

Several authors have reported on the growth of mixed $\text{Cu}(\text{In}_{1-x}\text{Ga}_x)\text{S}_2$ single crystals [25–30]. Bodnar et al. [27] have investigated the conditions of growth of solid $\text{Cu}(\text{In}_{1-x}\text{Ga}_x)\text{S}_2$ solutions by chemical vapor transport from a powder mixture of CuInS_2 and CuGaS_2 single crystals. Using differential thermal analysis they have constructed the phase diagram of the pseudo-binary CuInS_2 - CuGaS_2 -system and calculated the solidus and liquidus lines (Figure 3.5 (a)). As can be seen in the figure the order-disorder phase transitions of CuInS_2 are also typical for solid solutions of $\text{Cu}(\text{In}_{1-x}\text{Ga}_x)\text{S}_2$ with $x < 0.6$. On the basis of their experimental data they determined the heats of mixing in the liquid and solid phases (Figure 3.5 (b)). Although the heat of mixing was found to be positive (endothermic mixing) the critical temperature for limited solubility is ≈ 290 K. This is in agreement

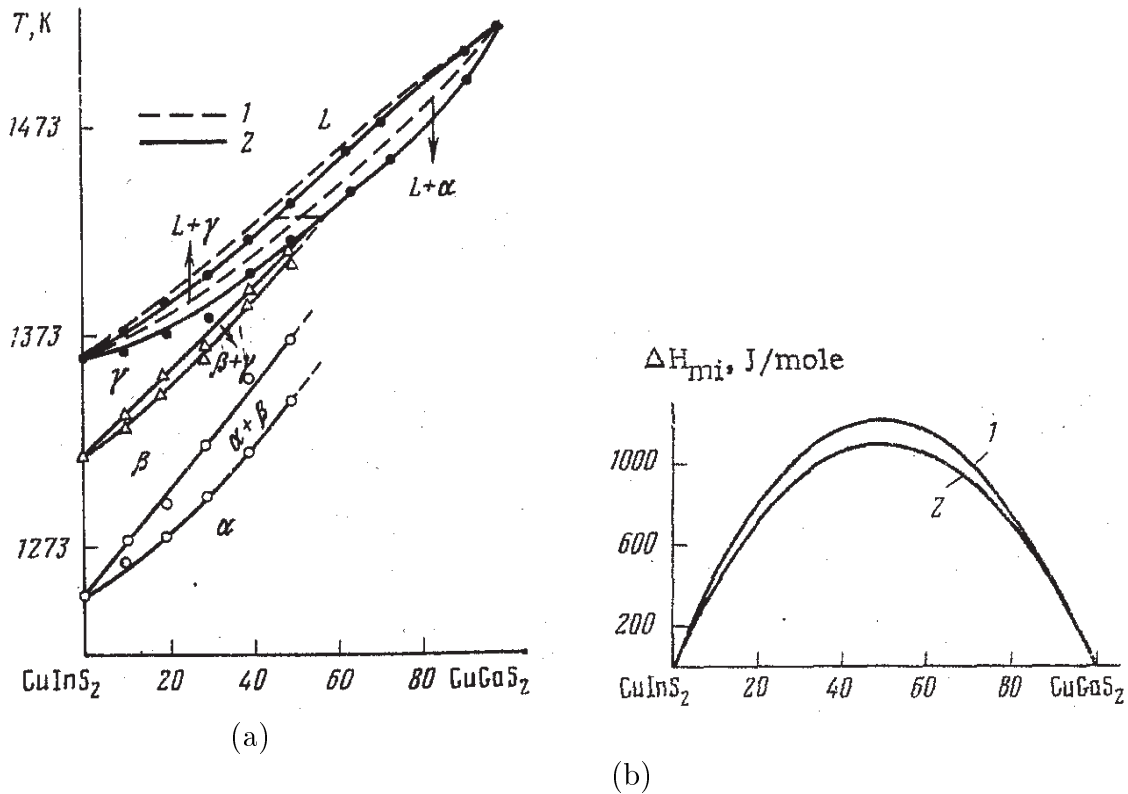


Figure 3.5: (a) Pseudo-binary phase diagram of CuInS₂-CuGaS₂ (α = chalcopyrite, $\alpha \rightarrow \beta$ = cation order-disorder transition, $\beta \rightarrow \gamma$ = cation-anion order-disorder transition) and (b) change in the heat of mixing in the CuInS₂-CuGaS₂ system in the solid (1) and liquid (2) phases, Ref. [27].

with theoretical calculations of Wei and Zunger [48]. They have calculated the mixing enthalpies of several mixed-cation CuMSe₂, $M = \text{Al, Ga, In}$ in chalcopyrite systems and found that the mixing enthalpy ΔH is positive and increases as the lattice mismatch increases. However, for most systems ΔH is rather small which suggest that they will be miscible in the whole composition range at finite temperature. Accordingly, the variation of the lattice constants a and c and the band gap energy with the composition of the solid solution obeys Vegard's law [25, 26, 28], i.e. there are no reports in literature on a miscibility gap in the CuInS₂-CuGaS₂ system.

The situation is different during crystal growth from the elements as there are several reports on CuGaS₂ growth from stoichiometric Cu-Ga-S mixtures under the presence of In [25, 30]. In these experiments In acts as a solvent only, resulting in Cu(In_{1-x}Ga_x)S₂ crystals with $x > 0.97$, which shows that CuGaS₂ formation is energetically favored over CuInS₂ formation.

Finally the above discussed results indicate that whereas stoichiometric mixtures of Cu-In-Ga-S form a quaternary Cu(In_{1-x}Ga_x)S₂ compound at finite temperatures, this is not

generally the case for non-stoichiometric mixtures of the elements where CuGaS₂ formation is preferential.

3.2.2 Equilibrium Considerations

One way of sketching the possible growth path during reactive annealing of the metallic precursors is to determine the equilibrium phase compositions at intermediate temperatures between room temperature and annealing temperature. Although this work mainly considers reactive annealing by rapid thermal processing where this temperature range is traversed in less than two minutes and therefore the system is likely to be far away from thermal equilibrium, such thermodynamic equilibrium considerations may still give valuable hints concerning the phase formation sequence during film growth.

In order to describe the thermodynamical state of a Cu-In-Ga-S system in an annealing furnace temperature, pressure and particle number may assumed to be constant. The thermodynamical variable which is best adapted to such a system is the Gibbs free energy

$$G = U - TS + pV = H - TS, \quad (3.1)$$

where U is the internal energy, T is the temperature, S is the entropy, p is the pressure, V is the volume, and H is the enthalpy. In equilibrium the Gibbs free energy is minimal, hence

$$dG = -SdT + Vdp + \sum_{i=1}^N \mu_i dN_i = 0, \quad (3.2)$$

where μ_i refers to the chemical potential of specimen i , and N_i is the number of particles of specimen i . Equation (3.2) has been numerical solved by means of the computer code *ChemSage* [113]. Enthalpy and entropy values for the binary and ternary compounds were either taken from a standard data base or in some cases theoretical estimations by Villora [107] were used. The formation of quaternary compounds has not been considered in this calculation. Further details can be found in [107].

The calculated equilibrium phase distribution of a Cu-In-Ga-S_x and a Cu-In-Ga-H₂S mixture with overstoichiometric amounts of Cu and S_x or H₂S at 25 °C, 450 °C and 550 °C are listed in Table 3.4. The equilibrium phase composition is influenced by the type of reactive atmosphere. In a Cu-In-Ga-H₂S mixture CuInS₂, CuGaS₂, and Cu₂S form under equilibrium conditions independent of temperature. If sulfur vapor is used as the reactive atmosphere the calculated equilibrium phase composition depends on temperature. Two phase transitions are predicted by the calculations:

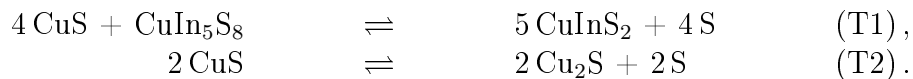


Table 3.4: Calculated equilibrium phase composition of a Cu-In-Ga-S_x and a Cu-In-Ga-H₂S system at various temperatures ($p = 1$ atm) (see also Ref. [107]).

Cu	In	Ga	S	$T =$	25 °C	450 °C	550 °C
1.2 mol	1.0 mol	0 mol	5 mol		0.2 mol CuIn ₅ S ₈ 1.0 mol CuS S _x	1.0 mol CuInS ₂ 0.2 mol CuS S _x	1.0 mol CuInS ₂ 0.1 mol Cu ₂ S S _x
1.2 mol	0.5 mol	0.5 mol	5 mol		0.5 mol CuGaS ₂ 0.1 mol CuIn ₅ S ₈ 0.6 mol CuS S _x	0.5 mol CuGaS ₂ 0.5 mol CuInS ₂ 0.2 mol CuS S _x	0.5 mol CuGaS ₂ 0.5 mol CuInS ₂ 0.1 mol Cu ₂ S S _x
Cu	In	Ga	H ₂ S	$T =$	25 °C	450 °C	550 °C
1.2 mol	0.5 mol	0.5 mol	5 mol		0.5 mol CuGaS ₂ 0.5 mol CuInS ₂ 0.1 mol Cu ₂ S H ₂ S H ₂	0.5 mol CuGaS ₂ 0.5 mol CuInS ₂ 0.1 mol Cu ₂ S H ₂ S H ₂	0.5 mol CuGaS ₂ 0.5 mol CuInS ₂ 0.1 mol Cu ₂ S H ₂ S H ₂

Transition temperatures are 420 °C for (T1) and 520 °C for (T2) at 1 bar. The transition (T2) can also be found in the Cu-S phase diagram (Appendix A.5) at $T = 507$ °C, $p = 1$ bar. These temperatures also depend on the process pressure. At 1×10^{-3} bar, which is a typical value for the process pressure during the reactive annealing step in sulfur vapor, the transition temperatures are lower by around 100 °C (Figure 3.6). The occurrence of these transitions does not depend on the $[Ga]/([In] + [Ga])$ ratio, i.e. they are also typical for a Ga-free Cu-In-S system with $[Cu]/([Cu] + [In]) > 1.0$. The effect of adding Ga to the system is merely the formation of the ternary CuGaS₂ phase which is stable over the entire temperature range between 25 °C and 550 °C regardless of the type of reactive atmosphere.

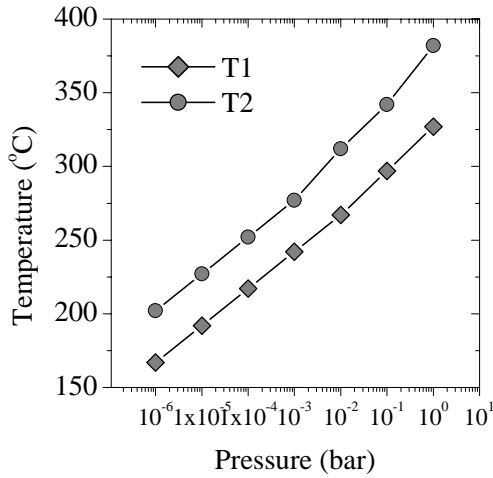


Figure 3.6: Calculated pressure dependence of transition temperature of transition T1 and T2.

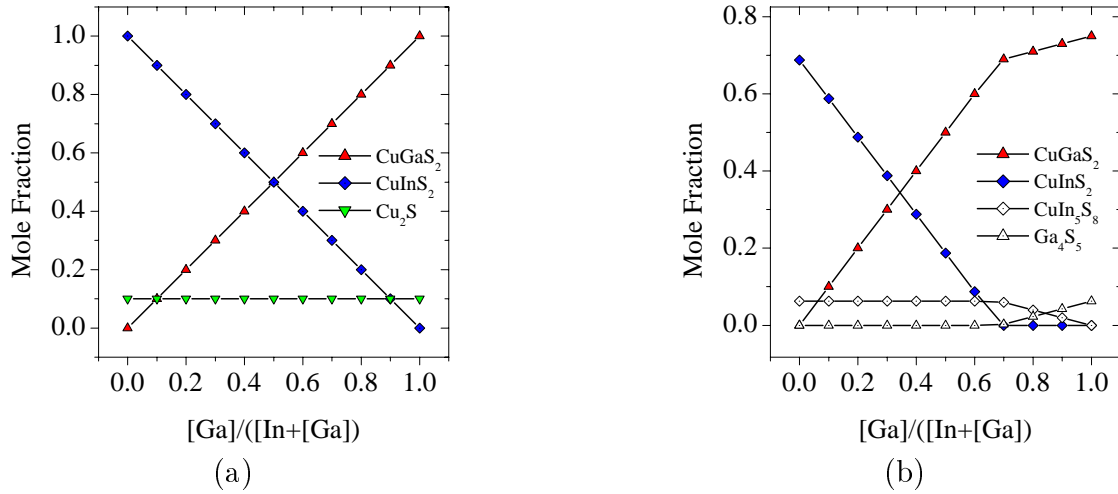


Figure 3.7: Equilibrium phase composition as a function of the $[\text{Ga}]/([\text{In}]+[\text{Ga}])$ ratio at $p = 1 \times 10^{-3}$ mbar and $T = 825$ K.

(a) Cu-rich system: $\text{Cu} = 1.2$ mol, $\text{In} = 1 \rightarrow 0$ mol, $\text{Ga} = 0 \rightarrow 1$ mol, $\text{S} = 5$ mol.

(b) In-rich system: $\text{Cu} = 0.75$ mol, $\text{In} = 1 \rightarrow 0$ mol, $\text{Ga} = 0 \rightarrow 1$ mol, $\text{S} = 5$ mol.

In a Cu-rich system the ratio of CuGaS_2 to CuInS_2 corresponds to the $[\text{Ga}]/([\text{In}]+[\text{Ga}])$ ratio of the system (Figure 3.7 (a)).

In a system with an overstoichiometric supply of In and Ga with respect to Cu the thermodynamically more stable ternary compound will form on excess of the less stable one. The situation is depicted in Figure 3.7 (b), which plots the equilibrium phase composition of a Cu-poor Cu-In-Ga-S system as a function of the $[\text{Ga}]/([\text{In}]+[\text{Ga}])$ ratio. As can be seen in the figure the amount of CuGaS_2 is equal to the amount of Ga in the system over the entire composition range (except $[\text{Ga}]/([\text{In}]+[\text{Ga}]) > 0.75$). Thus the Cu-deficiency of the situation only affects the In-containing compounds, by formation of the In-rich CuIn_5S_8 . As will be shown below the calculated phase behavior, which is in agreement with the preferential formation of CuGaS_2 observed in single crystal growth (Section 3.2.1), is also reflected in the phase formation sequence of $\text{Cu}(\text{In}_{1-x}\text{Ga}_x)\text{S}_2$ thin films.

The calculated phase compositions for the Ga-free system, as listed in Table 3.4, will confirm earlier experimental investigations of reactive annealing of metallic Cu-In films, reported by Binsma [33], Dzionk et al. [114], and Siemer [66]. Although the specific results depend on precursor deposition technique, stacking sequence, and reactive atmosphere all authors report certain critical temperatures for the formation of a single phase CuInS_2 film. At temperatures below this critical temperature the annealing step yields copper sulfides and solid solutions with a composition between In_2S_3 and CuIn_5S_8 but no CuInS_2 . The reported critical temperatures are in the range of 300°C to 375°C in the case of sulfur vapor and around 250°C in the case of H_2S as the reactive atmosphere. In sulfur vapor the critical temperature corresponds to the (T1) transition. In H_2S , where no critical temperature would be expected according to Table 3.4, the reported temperature is due

to the low dissociation constant of H_2S below the critical temperature resulting in small amounts of reactive sulfur, an effect which is not considered by the equilibrium calculations.

3.2.3 Phase Formation Sequence During Reactive Annealing of Cu-In and Cu-(In,Ga) Precursor Stacks

Ex-situ monitoring has been applied to investigate the phase formation sequence in the reactive annealing step of Cu-In and Cu-(In,Ga) precursors. Hereby the sulfurization process was aborted at different points during heat up or annealing. To assure that no major changes in phase composition will occur once the process is interrupted a rapid thermal processing (RTP) furnace has been used for this study. In such a furnace, where substrate heating is realized by an UV-lamp field, and where the thermal mass of the system is kept low, cool down ramps as fast as 5 K/s are possible in the temperature range between 500 °C and 200 °C. The process pressure was ≈ 1 mbar. Figure 3.8 shows the substrate temperature profile over time and indicates the points at which the process was interrupted. The PVD-deposited metal stacks had been stored for two to three days before being transformed to chalcopyrites. The atomic composition of all precursor layers was Cu-rich, i.e. $[\text{Cu}]/([\text{In}] + [\text{Ga}]) = 1.8$ and $[\text{Ga}]/([\text{In}] + [\text{Ga}]) = 0.3$.

Structural characterization and phase identification have been performed by X-ray diffraction (XRD) and depth-resolved Raman spectroscopy as described in Chapter 2. The layers were also examined by scanning electron microscopy (SEM).

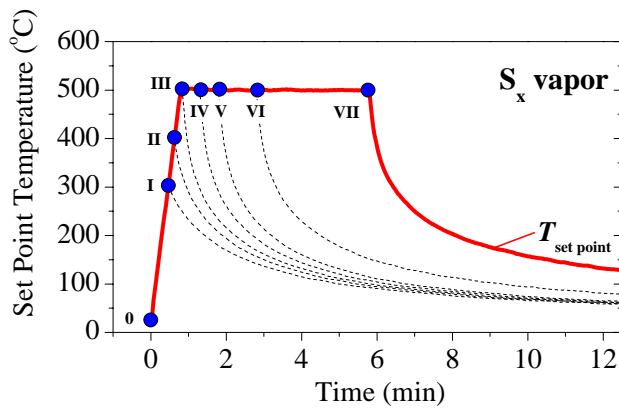


Figure 3.8: Temperature profile of S_x process. The labeled dots indicate the points where the sulfurization process was interrupted. A relation between set point temperature and actual substrate temperature is shown in Figure 2.4.

Cu-In precursors The results of the phase analysis by XRD and Raman are presented in Figure 3.9. As discussed in Section 3.1 after two days of storage Cu-In stacks mainly consist of Cu and CuIn_2 . During sample heat up precursor phase composition shifts from the In-rich binary phase CuIn_2 at room temperature to the Cu-rich binary phase $\text{Cu}_{11}\text{In}_9$ at elevated temperatures (point III). The chalcopyrite phase CuInS_2 already starts forming at point III, where the substrate temperature was ramped up to 500 °C and immediately cooled down. After annealing for another 60 s (point V) there are no metal phases anymore

and the secondary CuS phase can be found. X-ray diffraction in asymmetric mode and depth-resolved Raman measurements show that the CuS phase mainly segregates at the layer surface.

Cu-(In,Ga) precursors In Cu-(In,Ga) precursors Cu , CuGa_2 , and free In are the most prominent phases at room temperature. At the beginning of the heat up ramp In alloys to CuIn_2 and eventually to $\text{Cu}_{16}\text{In}_9$ (η' modification [103]) at higher temperatures. In contrast to the Ga-free series, samples at point III are still fully metallic and still contain free In . First sulfur containing phases, i.e. CuGaS_2 and CuIn_5S_8 , can be detected in sample IV. Thirty seconds later (point V) the layer is fully sulfurized and consists of CuGaS_2 , CuInS_2 , and CuS . With respect to the Ga-free case the formation of CuInS_2 is shifted to higher temperatures at a later stage of the annealing process.

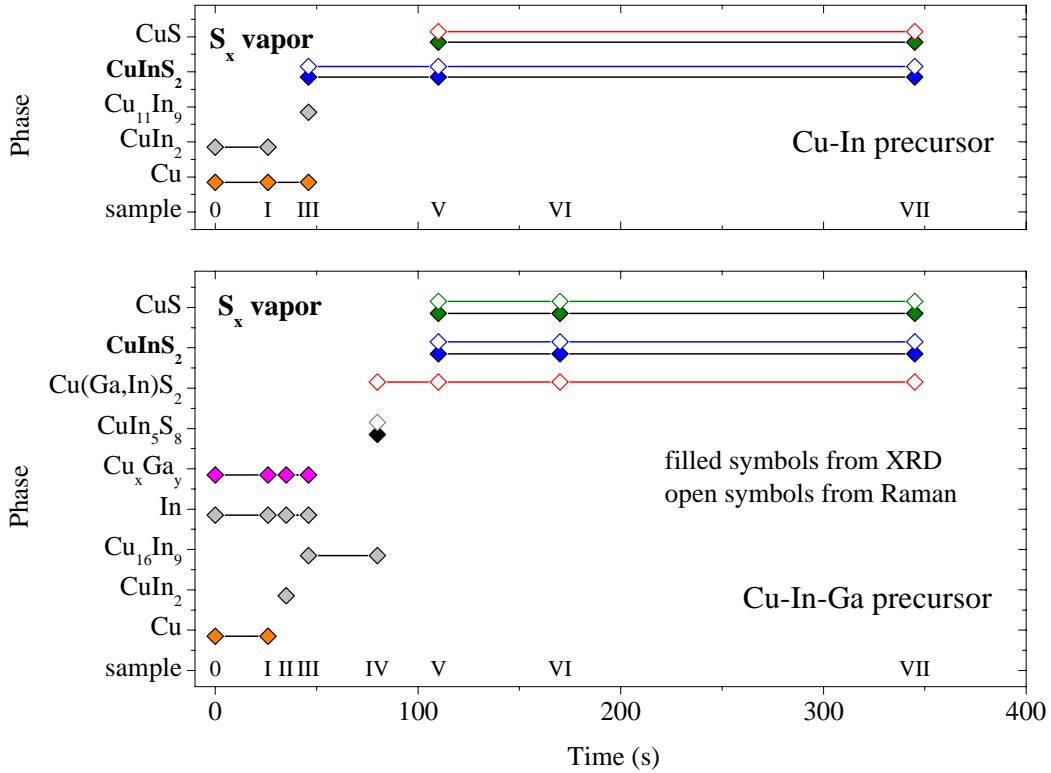
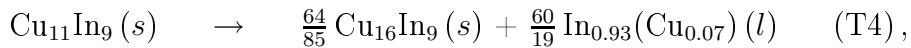
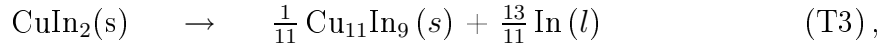


Figure 3.9: Phase formation sequence of Cu-In and Cu-In-Ga metal stacks when annealed in sulfur vapor as determined by XRD and Raman measurements. Samples are labeled according to Figure 3.8.

Growth path The major difference between the Ga-free sample series and the Ga-containing sample series is, beside the formation of the additional CuGaS_2 phase, that in

the former case the CuInS_2 phase is the first chalcogenide phase that occurs during reactive annealing whereas in the latter case an intermediate In-rich phase is observed before CuInS_2 segregation. The change in the phase formation sequence can be understood taking into account the precursor phase behavior.

As discussed in Section 3.1 at elevated temperatures the phase composition shifts from the In-rich binary phase to Cu-rich binaries, i.e.:



where the indexes (s) and (l) refer to solid and liquid phases respectively. Transition temperatures are $T_{\text{T1}} = 150^\circ\text{C}$ [102] and $T_{\text{T2}} = 300^\circ\text{C}$ [99] respectively. The excess, liquid In during these transitions either reacts with the excess Cu in the precursor by reactive diffusion or it reacts with the sulfur from the gas phase to form indium sulfide:



Since the $[\text{Cu}]/([\text{Cu}] + [\text{In}])$ ratio of the precursor is 1.8 all In can, in principle, be accommodated in the Cu-rich binary phases. Therefore kinetic aspects determine whether the released In reacts with the Cu in the precursor or with the sulfur from the gas phase. Indirect evidence for Cu-In alloying being favored to indium sulfid formation (T5) can be derived from the fact that substantial amounts of In_2S_3 would also lead to the formation of the volatile $\text{In}_2\text{S}(\text{g})$ thereby shifting the sample composition towards a higher Cu-excess [114]. However, no change in the $[\text{Cu}]/([\text{Cu}] + [\text{In}])$ ratio has been detected between precursor and sulfurized CuInS_2 film. Moreover, in the RTP system the chalcogen pressure builds up during sample heat up. As a result the chalcogen pressure is likely to be low at transition temperature T_{T3} and T_{T4} which avoids the formation of substantial amounts of indium sulfide.

Based on experimental results about the sequential growth of chalcopyrite thin films (see e.g. [33, 63, 96, 114–116]) two reaction paths can be distinguished in principle. On one hand the formation of the chalcopyrite by reaction from a metallic alloy, and on the other hand the occurrence of intermediate binary chalcogenide phases and the formation of the ternary phase via the binary phases. The growth paths may be referred to as direct and indirect, respectively.

The observed phase formation sequence of the Ga-free series shows that CuInS_2 is present already at an early stage of the reactive annealing process. Thus, it has to be concluded that the chalcopyrite compound forms directly from the Cu-In alloy. According to transition (T3) and (T4), which were derived from the equilibrium phase diagram, $\text{Cu}_{16}\text{In}_9$ is the only Cu-In alloy expected to be present in the precursor at temperatures above 300°C . Hence the direct growth path would read



However, according to the experimental results, in the case of reactive annealing of Cu-In bilayers no Cu₁₆In₉ has been observed, i.e. transition (T4) does not occur. Therefore, it has to be concluded that the CuInS₂ phase forms straight from the Cu₁₁In₉ phase



A growth path directly from the Cu₁₁In₉ phase also explains the delayed occurrence of detectable amounts of CuS with respect to the first detection of CuInS₂, since the amount of copper sulfide that forms according to transition (T6a) is almost ten times less than the amount of CuInS₂ formed, and still more than three times less than what would be expected according to (T6).

It has to be noted that the right hand side of (T6) and (T6a) contains Cu₂S as the secondary copper sulfide phase and not CuS which is the phase that is observed ex-situ at the samples at room temperature. However, as was discussed above, the CuS phase is not stable at film growth temperature but forms during sample cool down by sulfur adsorption from the gas phase, i.e. it is not involved in the film growth process.

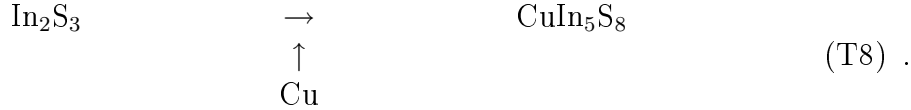
Due to the overall reaction times of less than 200 s needed to convert the entire layer to CuInS₂ an indirect growth path via binary sulphide phases seems to be less likely. Binsma [33] reports on indirect thin film CuInS₂ formation via interdiffusion of the binary sulfides, which proceeds at a much slower rate than the direct formation process. A finding also reported by Yamanaka et al. [117] who investigated reactive annealing of Cu-In layers with elemental Se. Thermodynamical equilibrium considerations by Cahen and Noufi [118] also support this, as they show that once the binary has formed, the thermodynamic driving force, i.e. the change in Gibb's free energy, from the binary to the ternary phase is very small. Experimental results on the phase formation sequence in reactive annealing of sputtered Cu-In precursors, reported by Siemer [66], also indicate a direct growth path. A reaction path way similar to (T6) was also proposed by Dzionk et al. [114].

In the case of Cu-(In,Ga) precursors the situation is different. Here the segregation of two chalcopyrite compounds is observed; one with a composition close to CuGaS₂ and one with a composition close to CuInS₂, whereby the Ga-rich* compound starts to segregate at an earlier stage of the annealing step than the In-rich compound. This behavior is on one hand due to the preferential formation of CuGaS₂ with respect to CuInS₂ as discussed in Section 3.2.2, and on the other hand due to the strong kinetic limitation of Cu-In alloying in Cu-(In,Ga) precursors which was shown in Section 3.1. The latter point is verified by the ex-situ monitoring data as unreacted In can be observed up to sample III (Figure 3.9), whereas a Cu-rich Cu-Ga alloy forms already at sample I. The Ga-rich chalcopyrite phase forms via a similar, direct growth path straight from the Cu-rich alloy:

*Here the terms "Ga-rich" and "In-rich" refer to the [Ga]/([In]+[Ga]) ratio and not to the [Cu]/([In]+[Ga]) ratio.



However, in the case of the In-rich compound a direct growth path according to transition (T6) is strongly suppressed. Instead unalloyed In leads to the segregation of In_2S_3 according to transition (T5), which then quickly transforms to CuIn_5S_8 by Cu-diffusion from the underlying Cu-In alloy.



The transition is likely to proceed very fast, since the crystal structures of In_2S_3 (defect spinel) and CuIn_5S_8 (spinel) are very closely related. The subsequent transition from CuIn_5S_8 to CuInS_2 , i.e.:

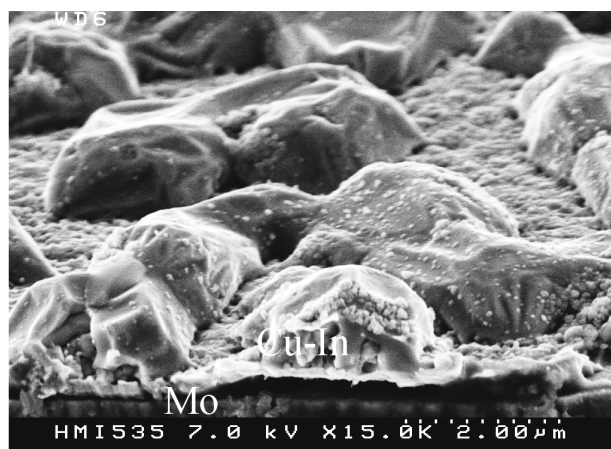


eventually delays the growth process with respect to the Ga-free case, as the transition involves the reorganization of In atoms, which occupy octahedrally coordinated sites in the spinel structure but tetrahedrally coordinated sites in the chalcopyrite structure. Here the sulfur sublattices retains its fcc structure apart from a change in lattice spacing during the phase formation [63].

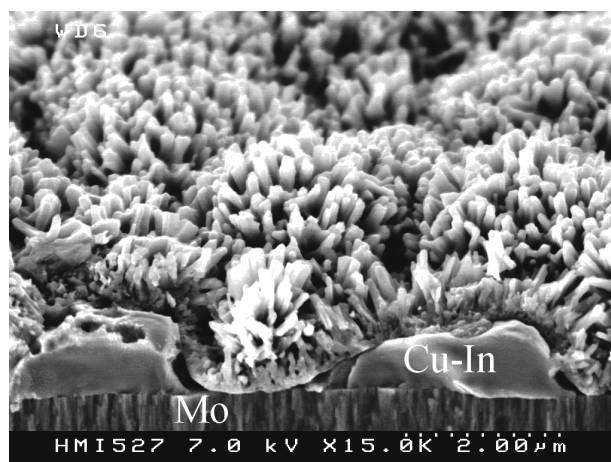
CuInS_2 formation in the case of Cu-(In,Ga) precursors via the outlined indirect path way is furthermore delayed because transition (T8) can only start after Cu_2S has been formed by (the kinetically delayed) reaction (T6).

As mention above the segregation of In_2S_3 can also lead to the formation of the volatile $\text{In}_2\text{S}(\text{g})$ phase. Indeed, there is a slight loss of Indium and the overall $[\text{Cu}]/([\text{In}] + [\text{Ga}])$ ratio of the sample decreases from ≈ 1.8 (precursor) to ≈ 1.6 (sulfurized film, point VII) as determined by ICP-AES.

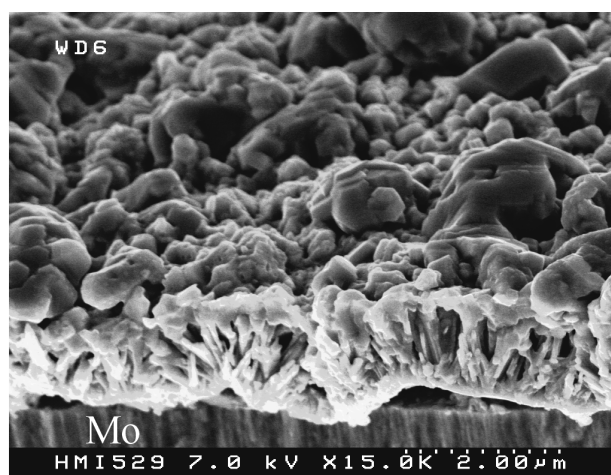
The intermediate formation of CuIn_5S_8 and the subsequent transition to CuInS_2 is also reflected in the morphology of the layer at the different points of the annealing step. Figure 3.10 shows SEM-images of cross sections of Cu-(In,Ga) samples annealed in sulfur vapor at 500 °C for 0 s, 30 s, 60 s, referring to point III, IV, and V in Figure 3.8. At point III (Figure 3.10 (a)) the layer still mainly consists of metallic phases and the typical precursor structure has remained unchanged. At the next stage (Figure 3.10 (b)) needle-shaped columnar grains have grown normal to the sample surface, a morphology which is typical for In-rich growth conditions [119]. Finally the formation of CuInS_2 and copper sulfide is reflected by the appearance of larger grains ($\approx 1 \mu\text{m}$) at the film surface (Figure 3.10 (c)). At this stage of the process voids start to form at the chalcopyrite/Mo interface.



(a) point III (500 °C, 0 s)



(b) point IV (500 °C, 30 s)



(c) point VII (500 °C, 60 s)

Figure 3.10: SEM-images of chalcopyrite formation from Cu-(In,Ga) precursors in sulfur vapor.

Reactive annealing in H₂S/Ar Besides reactive annealing in sulfur vapor an H₂S/Ar mixture has also been used for reactive annealing of Cu-(In,Ga) precursors. The equilibrium calculation presented in Section 3.2.2 predict in general a similar phase composition as in the case of sulfur vapor, except transition (T1) and (T2) are not expected to occur. For annealing in H₂S/Ar another RTP-system was used. The system mainly differs from the sulfur vapor system in the temperature profile used for sample heat up. Ex-situ monitoring has been applied to a series of samples. Figure 3.11 gives a schematic overview of the phases observed by XRD and Raman. Due to the slower ramp speed of 3 K/s in the H₂S/Ar, compared to 10 K/s in the sulfur vapor system, the metal phase transitions already took place when the process was interrupted at point I. At this stage of the process ($T_{max} = 325$ °C, no anneal) a compact chalcopyrite layer of composition Cu(In_{0.75}Ga_{0.25})S₂ (according to XRD and Raman peak position) can already be found, besides the metal phases Cu₁₆In₉ and free In. If the substrate temperature is ramped up to $T_{max} = 425$ °C CuInS₂ appears in addition to the Cu(In_{0.75}Ga_{0.25})S₂ layer. No Raman signal or XRD reflection of a Cu-S binary phase can be detected, although overall sample composition is Cu-rich, and AES depth profiles of the fully sulfurized samples indicate the segregation of Cu and S at the surface.

No intermediate In-rich phases can be observed during the incorporation of sulfur, although the phase composition of the Cu-(In,Ga) precursor is the same as in the series sulfurized in sulfur vapor. However, the presence of free In does not lead to the formation of an In-rich phase. This is not due to the faster heat up ramp used in the sulfur vapor RTP, as experiments using a more moderate heat up (2 K/s) also showed the CuIn₅S₈ phase at intermediate stages of annealing in sulfur vapor.

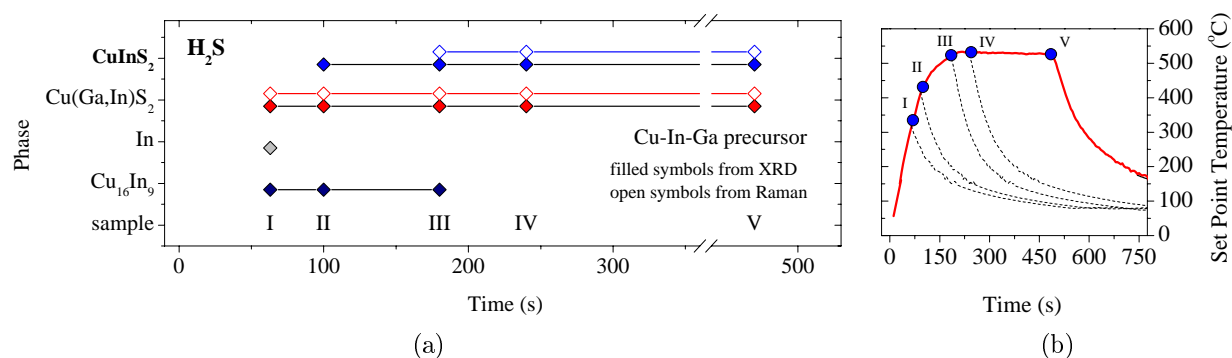


Figure 3.11: (a) Phase formation sequence of Cu-In-Ga metal stacks when annealed in H₂S/Ar as determined by XRD and Raman measurements. (b) Temperature profile of RTP furnace. Dots indicate points where process was interrupted.

The already discussed sequential segregation of a phase close to CuGaS₂ prior to CuInS₂ when annealing Cu-(In,Ga) precursors is also characteristic for samples sulfurized in H₂S/Ar. However, the growth path of the CuInS₂ phase proceeds via a more direct path in H₂S/Ar, i.e. the intermediate CuIn₅S₈ phase does not occur.

Conclusions On grounds of the presented data the following conclusion can be drawn. CuInS₂ thin film formation by annealing of Cu-In metal stacks in sulfur vapor using a rapid thermal processing proceeds via a direct phase formation path, i.e. no substantial amounts of binary phases segregate before CuInS₂ formation. The addition of Ga to the precursor stacks leads to the sequential segregation of CuGaS₂ and CuInS₂, whereby the CuGaS₂ phase forms prior to the CuInS₂ phase. If sulfur vapor is used as the reactive atmosphere the growths of the CuInS₂ phase is delayed with respect to the Ga-free case and the phase forms via an intermediate CuIn₅S₈ phase which is mainly due to large amounts of unalloyed In in Cu-(In,Ga) precursors.

3.2.4 Reactive Diffusion

In the previous section the phase formation sequence during reactive annealing of Cu-In and Cu-(In,Ga) precursors has been deduced from ex-situ monitoring data which allowed to identify the growth path of the thin film reactions involved in the growth process. However, as will be shown in this section kinetic aspects, such as initial nucleation at the precursor surface, the propagation of the chalcopyrite growth front, and diffusion of metal atom through the phases present in the film, greatly influence the final phase distribution in the sulfurized film. As a result the sulfurized absorber layers generally exhibit an inhomogeneous depth distribution of sulfurized phases. This section discusses the incorporation of sulfur in the metallic precursor layers on the basis of depth resolved Raman measurements and XRD measurements in asymmetric mode. A simple model for the thin film growth of the chalcopyrite layer by reactive diffusion of metal atoms will be proposed.

In the case of Cu-In precursors the CuInS₂ phase grows directly from the metal phase. CuInS₂ is the dominating chalcogenide phase present during the very first stage of sulfurization. As was shown in the previous section, once the annealing temperature of 500 °C has been reached the adsorbed sulfur from the vapor phase reacts with the Cu-In alloy to form CuInS₂. Let us now assume this nucleation phase quickly results in a homogeneous layer of CuInS₂ which covers the underlying Cu-In alloy. Then further reaction is not only controlled by the reaction rate of CuInS₂ formation but also by the various diffusion fluxes of Cu, In and S through the CuInS₂ layer. In general cation diffusion in Cu-chalcopyrites proceeds on a time scale orders of magnitude shorter than anion diffusion, i.e. atomic transport processes in the CuInS₂ lattice are characterized by mobile cations in a rigid anion sublattice. Atomic self diffusion coefficients of Cu and In in CuInS₂ single crystals are listed in Table 3.5. Since there was no report on the self-diffusion coefficient of S in CuInS₂ available data of S in CuGaS₂ and for Se in CuInSe₂ have been included for comparison. The higher cation mobility in Cu-chalcopyrites is mainly due to the fact that cation diffusion involves defects of the cation sub-lattice of very low formation energy [124]. On the other hand lattice defects which would act as diffusion path ways for anions, such as interstitial anions, anions at cation lattice points, or defects that involve local disordering of the anion sublattice have a very high formation energy. During film growth short circuit

Table 3.5: Self diffusion coefficient of Cu and In in CuInS₂, S in CuGaS₂, and Se in CuInSe₂.

	D (cm ² /s)	T (°C)	proposed diffusion mode	Ref.
Cu in CuInS ₂	$5.3 \times 10^{-9} - 3.3 \times 10^{-7}$	25	[V _{Cu}]	[120]
In in CuInS ₂	$1 \times 10^{-9} - 3.2 \times 10^{-7}$	650	[In _{Cu}][V _{Cu}]	[121]
S in CuGaS ₂	2×10^{-12}	700	interstitial S ₂	[122]
Se in CuInSe ₂	$2 \times 10^{-13} - 1 \times 10^{-12}$	700	[V _{Se}]	[123]

pathways for diffusion such as grain boundaries and/or surfaces are likely to enhance the atomic intermixing. Thus values for D in Table 3.5 represent a lower limit. Coming back to the thin film growth process, the higher cation diffusivity reported in literature, leads to the conclusion that once an homogeneous layer of the ternary chalcopyrite has formed on the metallic surface of the precursor further growth will proceed at the film surface, i.e. at the chalcopyrite - sulfur vapor interface. In other words, the flux of cations through the CuInS₂ layer supplies the surplus quantity of material in order to increase the thickness of the CuInS₂ layer.

Since the diffusion coefficient of In is much smaller than that of Cu at growth temperature the diffusional transport will be limited by In diffusion. Figure 3.12 schematically depicts the Indium concentration at a growth stage shortly after an initial layer of CuInS₂ has grown on top of the metal phase. Considering a flux of In atoms j_{In} across the CuInS₂ layer to the film surface the growth rate of the CuInS₂ layer, i.e. the rate of advance of interface II in Figure 3.12 is given by

$$c_{\text{II}} \left(\frac{dx}{dt} \right) = j_{\text{In}}. \quad (3.3)$$

Applying Ficks's First Law, i.e. $j_{\text{In}} = (-D \frac{\partial c}{\partial x})$, gives

$$\frac{dx}{dt} = \frac{1}{c_{\text{II}}} \left(-D \frac{\partial c}{\partial x} \right). \quad (3.4)$$

Assuming a linear change in concentration with distance within the CuInS₂ layer, i.e. $\frac{\partial c}{\partial x} = \frac{c_{\text{II}} - c_{\text{I}}}{d_{\text{CIS}}}$, where $d_{\text{CIS}} = \frac{dx}{dt}t$, one obtains

$$\frac{dx}{dt} = \sqrt{k \frac{1}{t}}, \quad \text{where} \quad k = \frac{D(c_{\text{II}} - c_{\text{I}})}{c_{\text{II}}}. \quad (3.5)$$

Integration of Equation (3.5) yields $x(t) = 2\sqrt{kt}$, i.e. the parabolic growth law of diffusion controlled reactive diffusion [125]. According to the experimental data presented in Section 3.2.3 in the case of Cu-In sulfurization in sulfur vapor a CuInS₂ layer of 2 μm

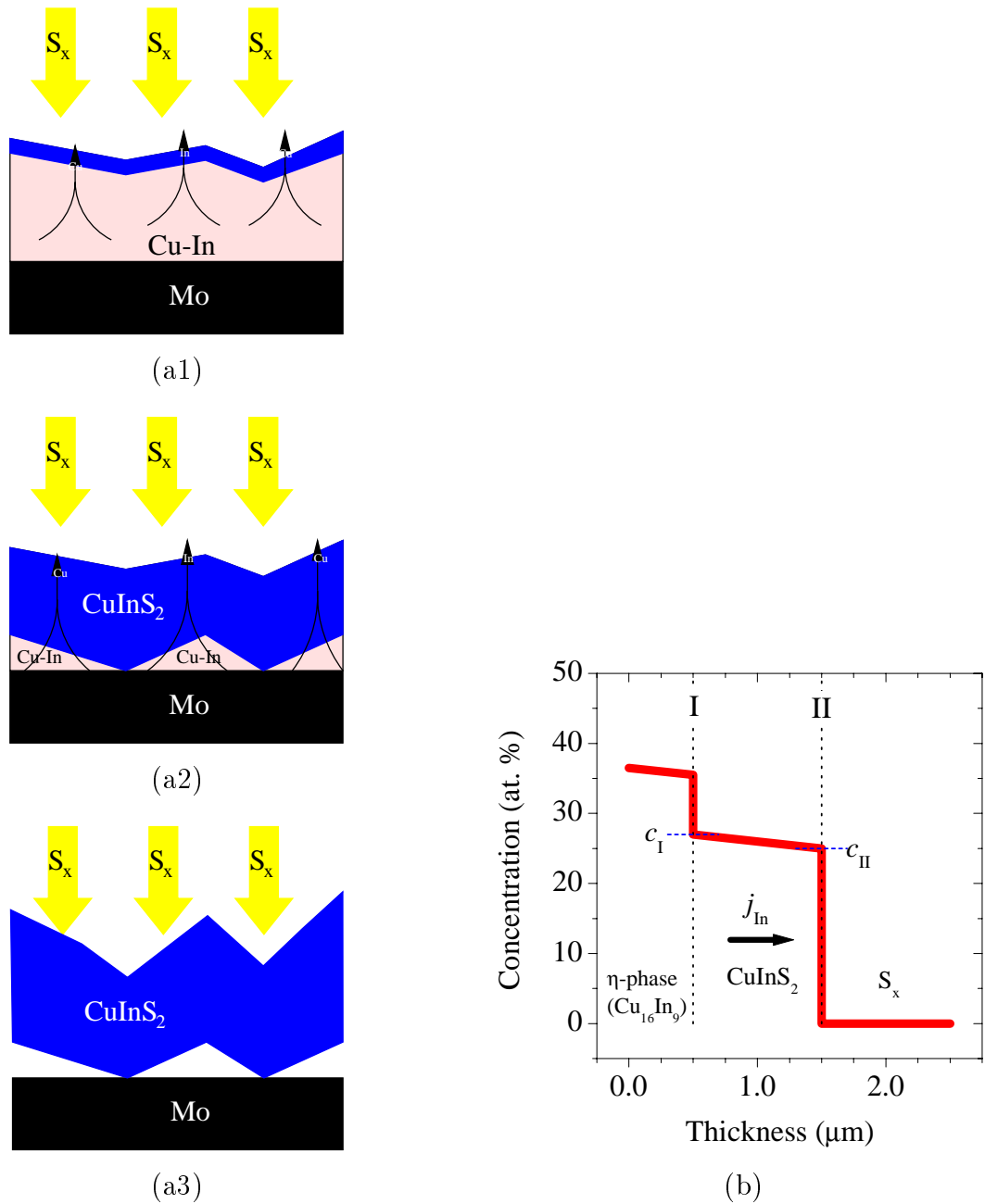


Figure 3.12: (a) Proposed model for the incorporation of sulfur by reactive diffusion. (a1) Formation of initial CuInS_2 layer at precursor surface. (a2) Diffusion of cations through CuInS_2 layer and reaction to CuInS_2 at sample surface (a3) Final layer. (b) Indium concentration in a $\text{Cu}_x\text{In}_y/\text{CuInS}_2/S_x$ layer at an intermediate stage of CuInS_2 layer growth (subfigure (a2)).

thickness has formed after about 60 s annealing time, which corresponds to a k -value of $3.3 \times 10^{-10} \text{ cm}^2/\text{s}$. The concentration gradient across the growing layer is given by the solubility of In in CuInS_2 . Assuming a solubility of 2 mol% In_2S_3 in CuInS_2 (Figure 3.4) gives a value of 0.04 for $(c_{\text{II}} - c_{\text{I}})/c_{\text{II}}$ and a D value of about $8.3 \times 10^{-9} \text{ cm}^2/\text{s}$. The latter value is in good agreement with the self diffusion coefficient of In given in Table 3.5, thus the assumption of a diffusion controlled growth mechanism is feasible with respect to the reported data for In diffusion in CuInS_2 . Due to the much higher Cu diffusivity in CuInS_2 (Table 3.5) the formation of CuInS_2 is likely to be paralleled by an accumulation of excess Cu atoms and subsequent formation of copper sulfide.

The proposed growth regime could be unambiguously verified by analyzing the sulfurization process of the Cu-(In,Ga) precursors. As discussed in the previous section, reactive annealing of Cu-(In,Ga) precursors is characterized by the sequential segregation of CuGaS_2 followed by CuInS_2 . A depth resolved phase analysis, realized by combining short Ar^+ sputter steps with Raman measurements (see Section 2.2.2.3) reveals that the observed sequential segregation of the two chalcopyrite compounds leads to an inhomogeneous Ga-depth distribution in the final layer. Figure 3.13 shows a series of Raman measurements performed at sample II (425 °C, 0 s), sample III (525 °C, 0 s) and sample V (525 °C, 300 s) of the sample series described in Section 3.2.3. Here the bottom spectra refer to surface measurements. Spectra measured after successive sputter intervals of equal length are vertically shifted along the y -axis of the plots. As can be seen in the figure at point II of the annealing step a $\text{Cu}(\text{In}_{1-x}\text{Ga}_x)\text{S}_2$ layer of $x \approx 0.75$ has overgrown the metallic precursor. The phase at the sample surface can clearly be identified by the strong $\text{Cu}(\text{In}_{1-x}\text{Ga}_x)\text{S}_2$ A1-mode which gradually disappears with increasing number of sputter intervals. At point III of the annealing step a second strong Raman mode appears in the near surface region which can be assigned to the A1-mode of CuInS_2 . This clearly shows that the second chalcopyrite phase starts to grow on top of the $\text{Cu}(\text{In}_{.25}\text{Ga}_{.75})\text{S}_2$ phase, hence the growth front for chalcopyrite formation is indeed located at the film surface. After 300 s of annealing the film is fully sulfurized and there is a distinct separation into a $\text{Cu}(\text{In,Ga})\text{S}_2$ phase at the back and a CuInS_2 phase.

The SEM images in Figure 3.13 also demonstrate that the segregation of chalcogenide phases is accompanied with the formation of voids. The number and the volume of these voids increases with the amount of copper sulfide which segregates during sulfurization, as could be verified by varying the $[\text{Cu}]/([\text{In}] + [\text{Ga}])$ ratio of the precursor. As can be seen in Figure 3.13 (a) at an early stage of the sulfurization process the layer consist of metallic hillocks or islands covered by an already sulfurized film. These metallic islands eventually lead to voids, once the cations have diffused into the sulfurized film, Figure 3.13 (b).

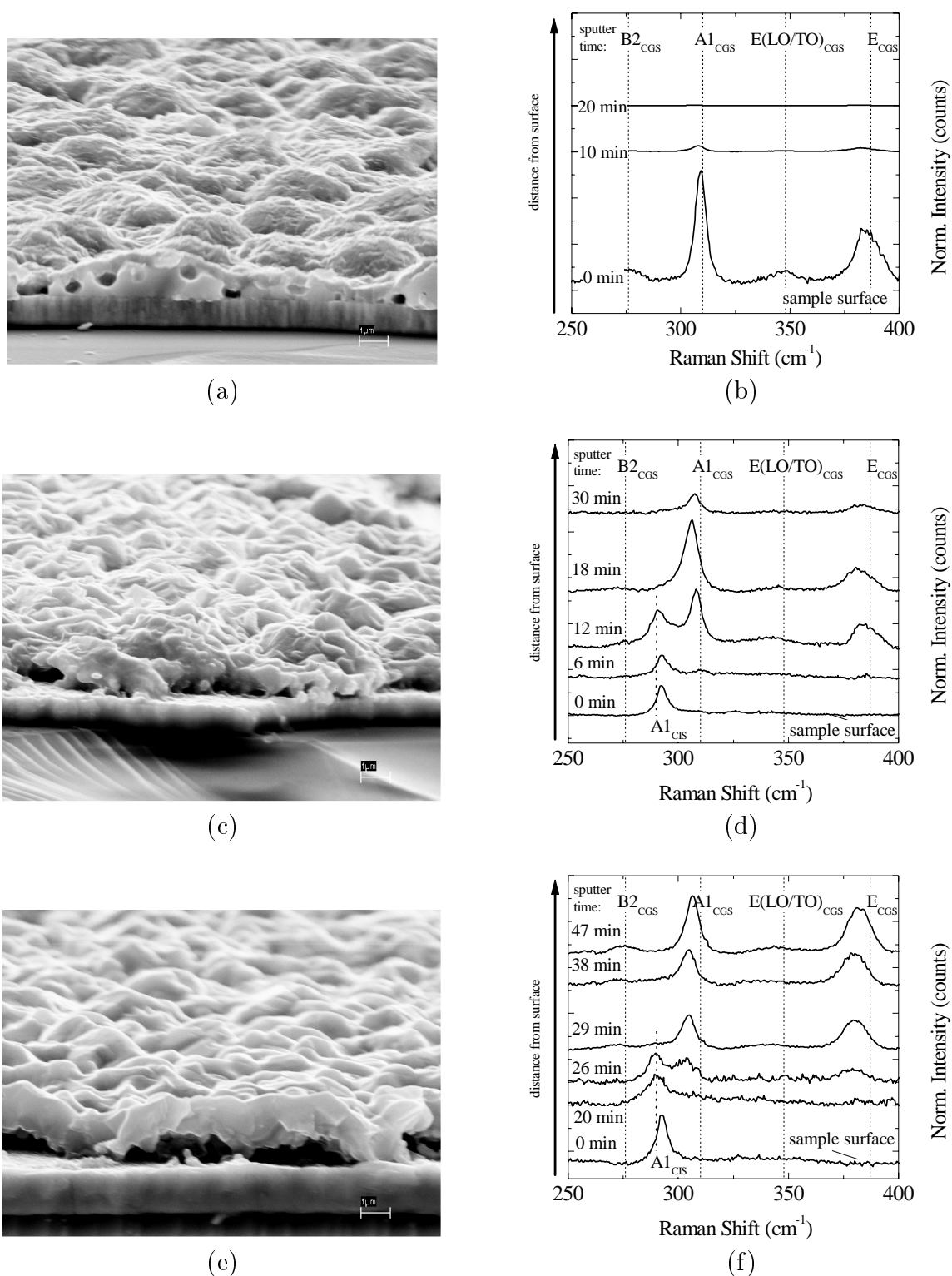


Figure 3.13: SEM images and depth resolved Raman measurements at $\text{Cu}(\text{In,Ga})$ precursors annealed in $\text{H}_2\text{S}/\text{Ar}$ for (a,b) 325°C , 0 s, (c,d) 425°C , 0 s and (e,f) 525°C , 300 s showing the sequential segregation of a CuGaS_2 phase (plot (b)) followed by a CuInS_2 phase (plot (c)) on top of the CuGaS_2 . Time labels at the Raman scans refer to cumulative sputter time.

The high cation mobility and the segregation of CuInS_2 on top of an already formed CuGaS_2 phase show that the incorporation of sulfur proceeds at the top surface of the multilayer system. The actual growth rate of the chalcogenide phase will be determined firstly by the rate of chemical reaction of Cu, In (or Ga) and S to form the chalcogenide phase at the film/sulfur vapor interface and secondly by the rate of diffusional transport of cations across the already formed layer. Assuming the former process, i.e. the rate of e.g. CuInS_2 formation is less than the flux of cations, an excess of these atoms would result, which can then be used to form layers of other phases such as binary sulfide phases. However, binary phases have not been observed in substantial amounts during CuInS_2 growth. Therefore, it is more likely to assume that the CuInS_2 growth rate is limited by diffusion.

The segregation of the In-rich phase on top of the already formed Ga-rich compound as observed in this work causes a highly inhomogeneous Ga-depth distribution in the final layer, where most of the Ga is located close to the Mo-back contact. Ga-accumulation at the back contact has also been reported for reactive annealing of Cu-In-Ga precursors in selenium vapor [37, 95, 126]. Braugner et al. [37] have assigned this to an reduced film formation velocity of CuGaSe_2 as compared to CuInSe_2 , determined by in-situ XPS and conductivity. However, as could be shown in this work, at least in the case of sulfur the reasons for the inhomogeneous Ga-depth distribution are twofold. Firstly the preferred formation of CuGaS_2 with respect to CuInS_2 leads to a sequential formation of the two ternary chalcopyrite compounds and secondly the location of the chalcopyrite growth front at the thin film surface are responsible for an inhomogeneous Ga-depth distribution typical for sequentially prepared $\text{Cu}(\text{In}_{1-x}\text{Ga}_x)\text{S}_2$ thin films. The influence of certain growth conditions such as substrate temperature during annealing and annealing time onto the final Ga-depth profile will be further discussed in Section 3.5 by means of sputter depth profiles. As will be shown in Chapter 4 the Ga-depth profile greatly influences the photovoltaic parameters of heterojunction solar cells processed from sequentially prepared $\text{Cu}(\text{In}_{1-x}\text{Ga}_x)\text{S}_2$ absorber layers.

3.3 Reactive Annealing - Recrystallization

Although all samples described in Section 3.2.3 are fully sulfurized shortly after the substrate temperature reaches the top temperature of the annealing step the crystal quality of the CuInS_2 top phase is still low at this stage. As will be shown in this section final film quality is only reached with ongoing annealing during which the layer undergoes a recrystallization step. The presence of the secondary copper sulfide phase during recrystallization turned out to be crucial in order to obtain device grade material. Furthermore in the case of Ga-containing layers the recrystallization step is accompanied by an In-Ga interdiffusion process between the CuInS_2 and the CuGaS_2 phase.

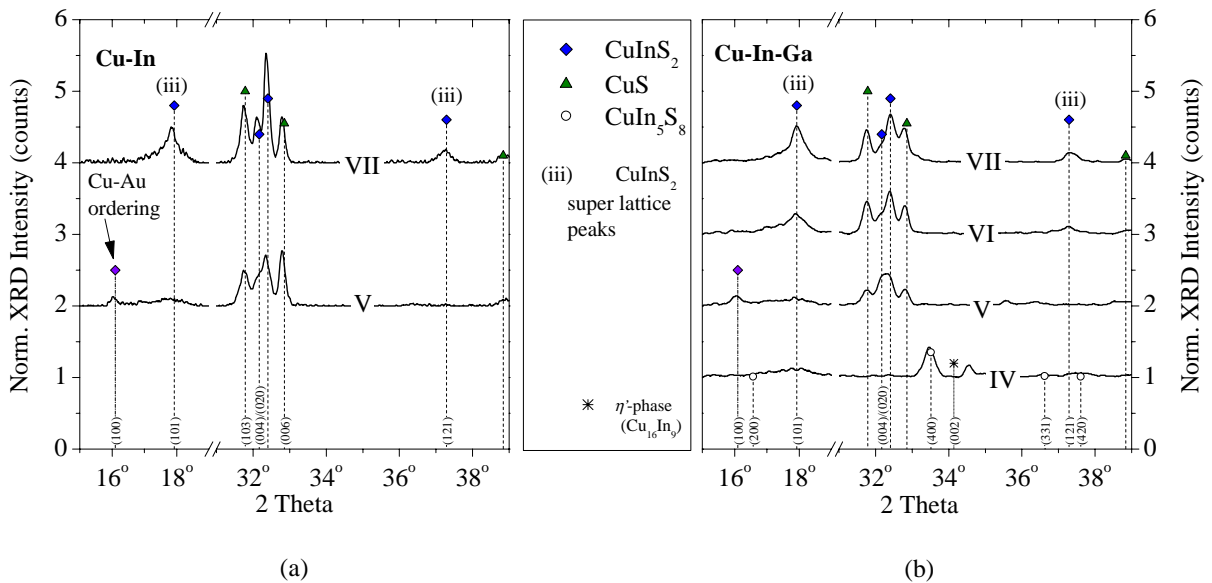


Figure 3.14: Sections of XRD spectra of Cu-In and Cu-In-Ga precursors annealed for different times. Samples are denoted according to Figure 3.8.

3.3.1 Cation-Ordering

Figure 3.14 shows a section of the XRD spectra of samples taken from the Cu-In and Cu-(In,Ga) series annealed for different times in sulfur vapor as described in Section 3.2.3. Although the peak splitting of the zincblende XRD reflections (group (i), see Section 2.2.4.1) can already be observed at samples annealed for only 60 s (point V, Figure 3.8), the peaks are still relatively broad which indicates very small undisturbed crystalline domains at this stage of the process. Typically values for the Full-Width-at-Half-Maximum (FWHM) are in the range of 0.1, which according to equation (2.8) refers to a grain size D below 85 nm. Furthermore, the absence of any chalcopyrite superlattice peaks indicates a high degree of disorder of the cation sublattice, i.e. chalcopyrite cation ordering has not been

fully achieved yet. Instead an additional reflection appears at 16.1° which can be assigned to the (100) lattice vector of the tetragonal unit cell. This reflection, which is forbidden for the chalcopyrite lattice, belongs to the group of superlattice reflections for a Cu-Au ordered lattice. Although, from a theoretical point of view, the energy of lattice formation favors a chalcopyrite ordered crystal [127] the phase has been observed several times in epitaxially grown Cu-chalcopyrite thin films [127–130]. The occurrence of Cu-Au ordering is not yet fully understood. Hunger [128] discusses its role as a metastable phase during film growth, based on experimental observations of epitaxially grown CuInS_2 thin films on Si. The appearance of the (100) XRD-reflection at an early stage of film growth, as observed in Figure 3.14, indicates that the phase may also play a role in multicrystalline film growth. Recent investigations of sequentially grown multicrystalline CuInS_2 thin films by Raman spectroscopy, reported by Álvarez-García et al. [131, 132], also point into this direction, as they revealed an additional Raman mode which was assigned to Cu-Au ordered crystal domains in the CuInS_2 lattice. According to Álvarez-García the additional *Cu-Au mode* is most pronounced in CuInS_2 films grown under Cu-poor ($\Delta m < 0$) conditions and/or at low annealing temperatures.

With increasing annealing time the layer recrystallizes resulting in larger crystal domains and a more perfectly ordered chalcopyrite lattice. In Figure 3.14 this is reflected by a decrease in FWHM of the zincblende CuInS_2 peaks (group (i)) to values around 0.05° ($\rightarrow D = 160 \text{ nm}$) and by the appearance of the chalcopyrite superlattice peaks. There is a significant increase in the intensity of the (101) reflection between sample V and sample VII both in Cu-In and in Cu-(In,Ga) samples, thus during annealing a substantial reorganization of the cation-sublattice has taken place. The recrystallization step is furthermore accompanied by an increase in morphological grain size (as determined by SEM) from typically 100 nm after 60 s of annealing to 1–2 μm after 300 s.

The presence of the binary copper sulfide compound was found to be crucial for recrystallization. This was experimentally verified by evaluating the integrated XRD intensities of the chalcopyrites superlattice reflections of samples with different amounts of CuS in the final sulfurized layer. Here the copper excess in the layer could be influenced by utilizing the observed characteristics of the thin film growth path (Section 3.2). As was already shown the release of unalloyed In during early stages of the reactive annealing step (transition (T3) in Section 3.2.3) can lead to the formation of volatile indium sulfides (transition (T5)), unless the free In alloys with the excess Cu in the precursor film (transition (T4)). Cu-In alloying is diffusion controlled, hence subject to a kinetic limitation. Therefore, assuming a constant sulfur pressure in the system fast heat up of the substrate temperature favors the formation and subsequent sublimation of InS and or In_2S_3 resulting in a higher Cu-excess in the final layer. As could be shown in Cu-(In,Ga) precursor layers Cu-In alloying is strongly suppressed, thus the effect is more pronounced in these films.

Metallic Cu-In and Cu-(In,Ga) precursor layers have been annealed in a CTP-furnace of constant sulfur pressure and the temperature gradient $\frac{\Delta T}{\Delta t}$ during sample heat up has been varied for different samples. Figure 3.15 shows sections of XRD-spectra of the final films. After reaching the top temperature of 500°C all samples have been annealed for 5 min.

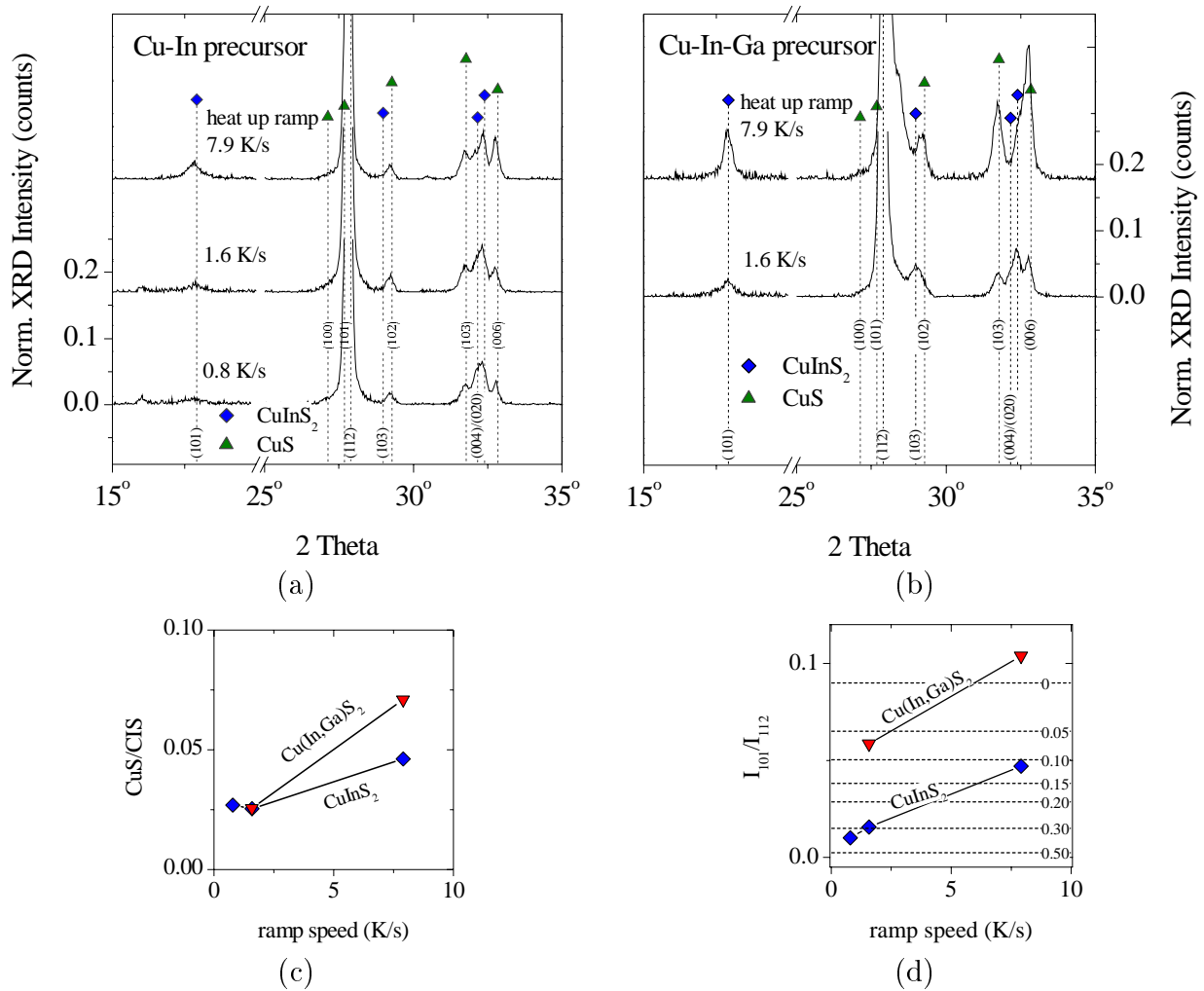


Figure 3.15: Upper Row: XRD intensity of the (011) chalcopyrite superlattice reflection of films sulfurized in sulfur vapor from (a) Cu-In precursors and (b) Cu-In-Ga precursors. After reaching the top temperature of 500 °C all samples were annealed for 5 min. Lower Row: Ratio of the integrated XRD intensities of (c) the secondary CuS phase over the chalcopyrite phase and (d) of the (101) superlattice reflection over the (112) zincblende reflection of the chalcopyrite phase. Dotted lines correspond to calculated $I_{(101)}/I_{(112)}$ ratios for different values of the cation disorder parameters δ_{disorder} (see Appendix A.1).

The spectra in the figure are normalized to the integrated intensity of the CuInS₂ (112) reflection so that the intensity of the CuS reflections serves as a relative indicator for the ratio of CuS to CuInS₂ in the film. The plots in the lower row of the figure compare the ratio of the integrated peak intensities of the CuS and the CuInS₂ XRD-reflections (subfigure (c)) and of the chalcopyrite (101) and the (112) reflection (subfigure (d)). The dashed horizontal lines refer to the expected intensity ratio as calculated for a CuInS₂ thin film of 2 μm thickness for different degrees of cation antisite disorder. The labels refer to the disorder parameter δ_{disorder} which corresponds to the ratio of antisite defects such as In_{Cu} to regularly occupied sites In_{In}. The disorder parameter and the calculations of corresponding XRD-intensities are discussed in Appendix A.1. As can be seen in subfigure (d) the amount of CuS in the sample correlates with the (101)/(112) ratio increase and thus with the degree of cation ordering of the recrystallized film.

3.3.2 In-Ga Interdiffusion

In case of Ga containing samples the reorganization of the cation-lattice during the recrystallization step is also accompanied by Ga-In intermixing between the CuGaS_2 layer at the back and the CuInS_2 layer at the top. The intermixing leads to a decrease in lat-

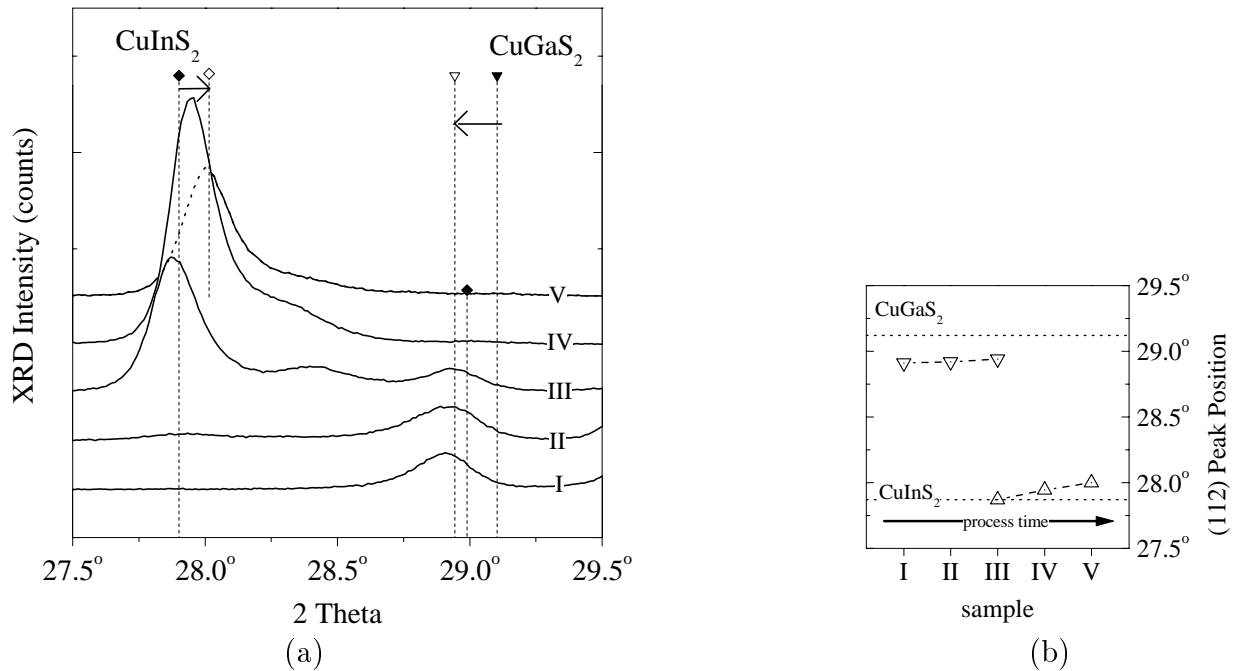


Figure 3.16: (a) CuInS_2 XRD 112 reflection shift with ongoing annealing in $\text{H}_2\text{S}/\text{Ar}$ and (b) Ga-content of top and back layer corresponding to the XRD peak position or Raman (see Figure 3.13) peak position.

tice constant of the CuInS_2 top layer, which is reflected by a shift of the position of the XRD reflections. Figure 3.16 (a) shows the (112) reflection of the top layer with ongoing annealing in $\text{H}_2\text{S}/\text{Ar}$ (Section 3.2.3). The shift of the XRD reflection corresponds to an incorporation of $\approx 10\%$ of Gallium into the top phase. A systematic variation of several growth parameters revealed that the degree of intermixing mainly depends on the temperature during annealing and on the amount of copper sulfide during annealing (further details will be given in Section 3.5).

Plot III in Figure 3.16 shows an additional XRD-reflection at around 28.45° . As could be deduced from additional reflections at higher angles this reflection is the strongest reflection of an additional cubic phase in the layer. Asymmetric XRD-scans of sample III revealed that this phase is located inbetween the CuInS_2 top phase and the CuGaS_2 phase at the back (Figure 3.17). With decreasing angle of incidence Φ the measurement becomes more surface sensitive (Figure 2.11) and, due to the layered structure of the film, the relative intensity of the CuGaS_2 reflection at 29.0° decreases. Subfigure (b) indicates that the cubic phase is located on top of the CuGaS_2 phase. The cubic phase can be assigned to

a $\text{Cu}(\text{In}_{1-x}\text{Ga}_x)\text{S}_2$ phase with $x \approx 0.5$ of the cubic sphalerite structure. The phase seems to be a metastable phase during film growth, since its contribution to the XRD-spectra decreases with ongoing annealing time (Figure 3.16), accompanied by the observed peak shift of the top phase.

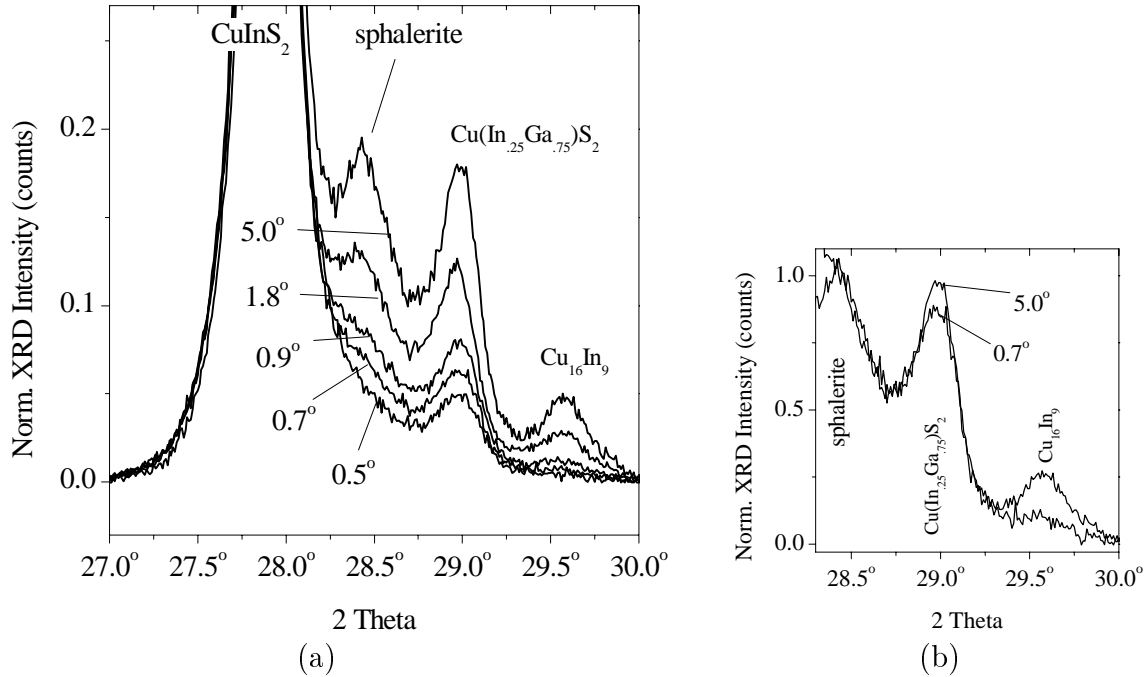


Figure 3.17: Asymmetric XRD-scan of a Cu-(In,Ga) precursor sulfurized in $\text{H}_2\text{S}/\text{Ar}$ (sample III of series (ii), $T_{\text{max}} = 525^\circ\text{C}$, no annealing). Labels denotes the angle of incidence Φ . All scans are normalized (a) to the (112) intensity of the CuInS_2 top layer or (b) to the intensity of the sphalerite contribution at 28.45° .

Ga-In intermixing turned out to be the decisive mechanism during film growth with respect to the $[\text{Ga}]/([\text{In}] + [\text{Ga}])$ surface composition of the absorber layer, which in turn determines the photovoltaic parameters of a heterojunction solar cell processed from such a layer. The influence of precursor Ga-content, sulfurization time, and sulfurization temperature onto the Ga depth profile of the absorber layer will be further discussed in Section 3.5.

3.3.3 Tentative Explanation for Cu_{2-x} Induced Recrystallization

As discussed above the reorganization of the cation sublattice during recrystallization, benefits from the presence of an additional copper sulfide phase. This paragraph proposes a tentative model for the recrystallization process on grounds of the phase behavior of the Cu₂S-In₂S₃ system, i. e.: (i) the solubility of CuInS₂ in Cu₂S at elevated temperatures and (ii) the structural similarities between Cu₂S and CuInS₂.

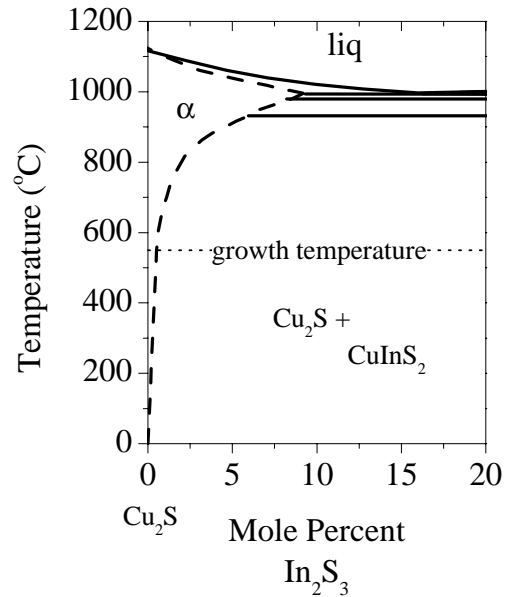


Figure 3.18: Section of the Cu₂S-In₂S₃ pseudo-binary phase diagram between 0 mol % and 20 mol % In₂S₃ showing the high solubility of CuInS₂ in Cu₂S at elevated temperatures.

As can be seen from the Cu₂S-In₂S₃ phase diagram given by Figure 3.4 [111] at high temperatures ($T > 800^\circ\text{C}$) the homogeneity region of the α -phase, which describes the region of solubility of CuInS₂ in Cu₂S, is rather broad (equivalent to ≥ 10 mol % In₂S₃), whereas at room temperature the homogeneity region of the phase is small. When extrapolating the phase boundary of the α phase to lower temperatures, it can be concluded that the solubility of CuInS₂ in Cu₂S at 550 °C is still ≥ 1 mol % (Figure 3.18). At growth temperature, when a fully sulfurized film consists of CuInS₂ grains and Cu₂S, some of the CuInS₂ will be dissolved in the secondary phase. During sample cool down the CuInS₂ solubility decreases and the ternary compound precipitates in the Cu₂S grains or, more likely, at the CuInS₂/Cu₂S phase boundaries. Dendritic CuInSe₂ precipitates in the Cu₂Se phase region of a CuSe₂/CuInSe₂ diffusion couple annealed at 550 °C for several hours were reported by Park et al. [133]. The solubility of CuInSe₂ in Cu₂Se is very similar to the Cu₂S/CuInS₂ phase system. Although Park et al. do not discuss the effect in terms of the α -phase region of the phase diagram, their experimental observation clearly indicates the non-zero solubility of the chalcopyrite phase in the Cu₂Se secondary phase. Furthermore they observed a decreased density of precipitates near the Cu₂Se/CuInSe₂ phase boundary of the diffusion couple, which indicates that in this region of the sample the dissolved ternary compound segregates at the phase boundary itself.

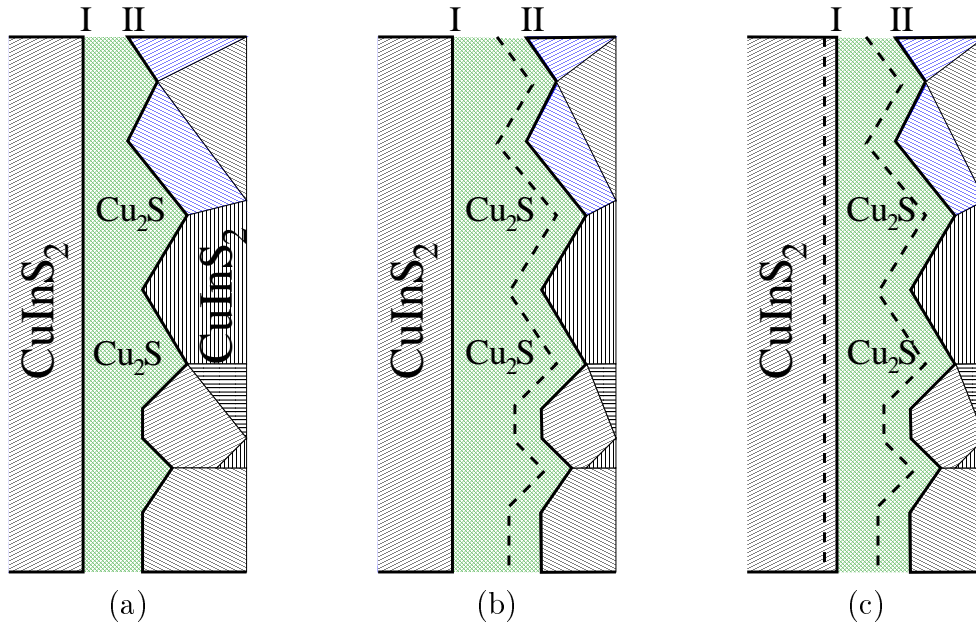


Figure 3.19: Recrystallization of a CuInS_2 thin film by a moving Cu_2S layer.

Based on these considerations on one hand and on the experimental results collected in the course of this work on the other hand the following tentative model for film recrystallization will be proposed. Assuming that small and highly structural defected grains generally show a higher solubility a growth regime which provokes the continuous dissolution and precipitation of the CuInS_2 phase at $\text{CuInS}_2/\text{Cu}_2\text{S}$ interfaces will eventually lead to a recrystallized film of improved structural quality. The situation is schematically depicted in Figure 3.19. Subfigure (a) shows two CuInS_2 regions separated by a thin layer of Cu_2S . The region on the left hand side (interface I) may be of chalcopyrite structure and may be significantly larger in grain size than the region on the right hand side (interface II). At the next stage (subfigure (b)) the Cu_2S layer starts to extend into the right hand side region due to the assumed higher solubility of the defected CuInS_2 phase at interface II. Once the Cu_2S is supersaturated with In CuInS_2 will precipitate, which will preferably occur at the region of lowest solubility, i.e. at interface I (subfigure (c)). Since the precipitation lowers the In concentration in the intermediate layer dissolution of CuInS_2 at interface II will proceed. As a result the Cu_2S layer will move into the *low quality* region leaving a recrystallized growing grain of CuInS_2 behind. The process will eventually terminate at boundaries of CuInS_2 grains of similar size and structure.

The atomic exchange processes at the $\text{CuInS}_2/\text{Cu}_2\text{S}$ interface can also be understood from a structural point of view. At typical growth temperatures ($\approx 550^\circ\text{C}$) Cu_2S crystallizes in a cubic fcc structure, usually referred to as digenite (see Cu-S phase diagram in Appendix A.5). Figure 3.20 gives an illustration of the crystal structure in comparison to the chalcopyrite structure. As can be seen in the figure both structure have the same chalcogen lattice. The lattice constant of Cu_2S is with $a_{\text{Cu}_2\text{S}} = 0.557 \text{ nm}$ [99] only slightly higher than that of CuInS_2 , $a_{\text{CuInS}_2} = 0.5523$. All 16 tetrahedral sites in the double unit cell of

Cu₂S in Figure 3.20 (a) are occupied by Cu atoms, whereas in the chalcopyrite structure 8 sites remain unoccupied and the other 8 are occupied by 4 Cu and 4 In atoms respectively. Since the digenite phase is slightly Cu-poor with respect to an ideal Cu₂S lattice some of the Cu-sites will be unoccupied, thereby opening diffusion paths for In in Cu_{2-x}S.

As was shown in the previous section recrystallization proceeds at a time scale of only a few minutes. Annealing times as short as 300 s are sufficient to fully recrystallize a layer with a thickness of 2 μm. According to the proposed model this implicates that the assumed Cu₂S layer propagates through a CuInS₂ grain at a velocity of $\approx 1 \times 10^{-6}$ cm/s. In order to check whether this values is feasible at all the required concentration gradient in the intermediate Cu_{2-x}S layer can be estimate as follows.

The driving force for ongoing recrystallization is the difference in solubility at interface I and II which will lead to a gradient $dc_{\text{In}}^{\text{Cu}_2\text{S}}/dx$ of the In concentration in the Cu₂S phase. The resulting flux j_{In} , assuming Fick'-ian diffusion, will be $j_{\text{In}} = D_{\text{In}}dc_{\text{In}}^{\text{Cu}_2\text{S}}/dx$. In turn, this flux determines the growth rate at interface I, i.e. $j_{\text{In}} = c_{\text{In}}^{\text{CIS}} \frac{\Delta x}{\Delta t}$, where $c_{\text{In}}^{\text{CIS}}$ refers to the concentration of In in the CuInS₂ phase and $\frac{\Delta x}{\Delta t}$ is the velocity of propagation of interface I. It follows

$$\frac{\Delta x}{\Delta t} = \frac{D_{\text{In}}}{c_{\text{In}}^{\text{CIS}}} \frac{dc_{\text{In}}^{\text{Cu}_2\text{S}}}{dx} \quad (3.6)$$

Assuming a diffusion coefficient of $D_{\text{In}} = 10^{-8}$ cm²/s (see Table 3.1) and a Cu₂S layer thickness d of 10 nm and simplifying dc/dx to $\Delta c/d$ yields

$$\frac{\Delta x}{\Delta t} \approx 10^{-2} \left(\frac{\Delta c_{\text{In}}}{c_{\text{In}}^{\text{CIS}}} \right). \quad (3.7)$$

Hence, to realize a propagation velocity of $\approx 1 \times 10^{-6}$ cm/s for a 10 nm thick Cu₂S layer, which corresponds to the dissolution and subsequent segregation of a CuInS₂ layer of 2 μm thickness, the concentration gradient $\Delta c/c^{\text{CIS}}$ imposed by the difference in solubility of the CuInS₂ phase at interface I and II, would have to be $> 10^{-4}$. Taking into account

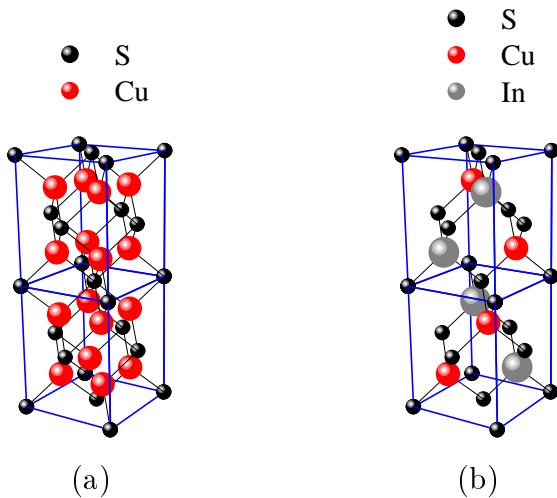


Figure 3.20: Crystal structure of (a) Cu₂S (digenite) and (b) CuInS₂. Note the identical anion sublattice.

the absolute solubility of CuInS_2 in Cu_2S of 10^{-2} the estimated value of 10^{-4} is relatively small. Thus, based on literature values for the In-diffusion coefficient the proposed recrystallization mechanism via a reorganization of the cation lattice by a moving intermediate Cu_2S can well proceed in the experimentally observe time scale of a few minutes. Although the phase transition discussed in the proposed model are solid state transitions (due to the high In-mobility in the secondary phase) the secondary phase can be imaged to act like a “quasi-liquid” flux agent which effectively recrystallizes the film.

3.4 Growth Model

The experimental results concerning sulfurization of evaporated Cu-In and Cu-(In,Ga) precursors will be summarized in the following. Figure 3.21 demonstrates the observed phase formation sequence in a schematic overview.

On the basis of the experimental results the thin film growth process can be divided into three stages:

- precursor alloying
- incorporation of sulfur
- recrystallization

In the case of Cu-In precursors the CuInS_2 phase grows directly from the metallic phase of the alloyed precursor. The chalcopyrite CuInS_2 is the only chalcogenide phase present during the first stage of sulfurization. This is mainly due to the rapid ramp up of the substrate temperature which assures that the critical temperature of CuInS_2 formation is quickly reached thereby effectively avoiding the formation of CuIn_5S_8 which, according to phase equilibrium calculations is the more stable ternary phase at temperatures below 400°C . Once the annealing temperature of 500°C has been reached the adsorbed sulfur from the vapor phase reacts with the Cu_xIn_y alloy to form CuInS_2 at the precursor surface. It could be shown that the chalcopyrite growth front is located at the thin film surface, thus further growth of CuInS_2 will proceed at the layer surface by reaction diffusion of Cu and In through the already formed CuInS_2 layer. The reactive diffusion of the metal atoms which depletes the precursor layer underneath the already formed CuInS_2 also explains the formation of voids with ongoing annealing time. Parallel to the segregation of CuInS_2 the formation of the secondary copper sulfide phase is expected, however according to ex-situ monitoring experiments detectable amounts of copper sulfide were only found shortly after the CuInS_2 phase starts to form. During sample cool down the Cu_2S phase transforms to CuS . The addition of Ga to the precursor stack leads to changes in the phase composition of the metallic precursor. Whereas Cu-Ga binary phases already form during or shortly after precursor deposition the alloying of Cu-In is strongly suppressed. Experiments have shown that a Cu-Ga phase at the interface between Cu and In effectively avoids any Cu-In phase formation, even after month of precursor storage. As a consequence almost all

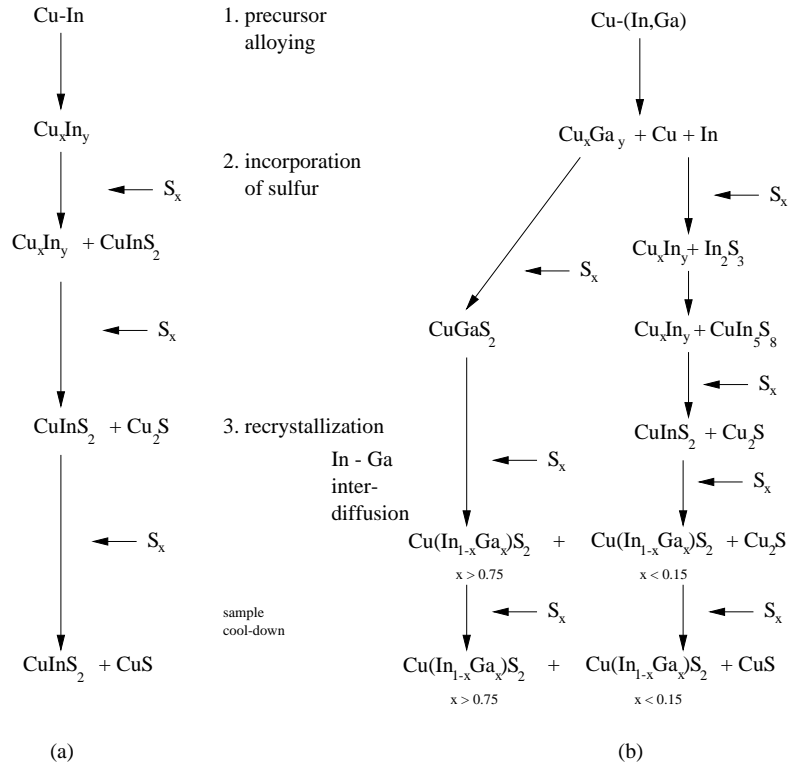


Figure 3.21: Schematic overview of phase formation sequence during reactive annealing of (a) Cu-In and (b) Cu-In-Ga precursors in sulfur vapor.

In in a Cu-(In,Ga) samples is still unalloyed at the beginning of the reactive annealing step. In general the sulfurization of Ga-containing precursor leads to the segregation of two ternary compounds with compositions close to CuGaS_2 and CuInS_2 respectively. The CuGaS_2 phase grows directly from Cu-Ga alloys in the precursor. Regardless of the type of reactive atmosphere the phase forms prior to the CuInS_2 phase, which is in agreement with the presented thermodynamical equilibrium calculations. In the case of reactive annealing in sulfur vapor the growth path of the CuInS_2 phase is furthermore shifted to a more indirect path. This is mainly due to the fact that, as mentioned above, most of the precursor surface is still covered by unalloyed In which prevents a direct formation path. Instead, the In-rich surface composition leads to the segregation of In_2S_3 which then easily transforms to CuIn_5S_8 . Since the transition from the CuIn_5S_8 phase to the CuInS_2 top phase involves the reorganization of In atoms in the crystal lattice the growth process is delayed with respect to the Ga-free case.

Once the films are fully sulfurized they undergo a recrystallization process which is characterized by an increase in morphological grain size and an improvement in chalcopyrite cation ordering. The recrystallization step, which is typically for both Ga and Ga-free samples, is induced by the presence of Cu_2S during film growth. A direct comparison of Ga-free and Ga-containing samples revealed an additional beneficial effect of Ga on the degree of cation ordering as can be judged by comparing the chalcopyrite superlattice

peaks. In Ga-containing films the recrystallization stage is furthermore accompanied, by interdiffusion of Ga and In between the ternary phases which leads to two quaternary $\text{Cu}(\text{In}_{1-x}\text{Ga}_x)\text{S}_2$ compounds of composition $x < 0.15$ and $x > 0.75$ respectively.

3.5 Gallium Depth Distribution

The ex-situ growth monitoring experiments described in Section 3.2.3 revealed that the reactive annealing process of Cu-(In,Ga) precursors is characterized by the sequential segregation of CuGaS₂ and CuInS₂. It was furthermore shown that the sequential segregation leads to an inhomogeneous Ga-depth distribution where the CuInS₂ phase is located on top of the CuGaS₂ phase. During the recrystallization stage of the film growth sequence Ga-In intermixing takes place, which eventually changes the composition of the top phase from pure CuInS₂ to Cu(In_{1-x}Ga_x)S₂. For heterojunction formation it is the top phase which mainly influences the material properties that are important for the current transport at the junction, such as the energetic position of valence and conduction band, the band gap energy, carrier densities, and defect densities. Therefore the study of the Ga-depth profile was one of the major aims of this thesis in order to (i) understand the underlying atomic transport mechanism and (ii) to deliberately influence the concentration of Ga at the interface in Cu(In_{1-x}Ga_x)S₂/CdS/ZnO hetero-junction solar cells. This section discusses the influence of precursor composition, i.e. the $[Ga]/([In] + [Ga])$ ratio, and sulfurization temperature and time onto the Ga-depth profile and in particular onto the composition and the structural properties of the top phase. By means of sequentially prepared CuGaS₂/CuInS₂ thin film diffusion couples effective values for the chemical diffusion coefficient of Ga in CuInS₂ thin films and In in CuGaS₂ thin films will be determined.

Three characterization techniques were employed for Ga-depth profiling: 1. secondary neutral atom mass spectrometry (SNMS), 2. depth-resolved Raman spectroscopy, 3. asymmetric XRD-measurements with varied angles of incidence. The techniques were already discussed in Chapter 2.

3.5.1 As Grown Cu(In_{1-x}Ga_x)S₂ Layers

SNMS Figure 3.22 (a) shows a typical depth profile of a Ga-containing absorber film. The layered structure of the sample with CuInS₂ at the top and with CuGaS₂ close to the Mo/glass substrate can clearly be recognized. The maximum of the Cu and S signal near the sample surface indicates the segregation of the secondary Cu-S phase at the surface. The depth profiles are significantly broadened which originates from resolution limitations of the SNMS technique, as discussed in Section 2.2.1, and more importantly from sample related effects such as interface and surface roughness and microscopic non-uniformities of thickness and composition. A rough measure of the degree of broadening is given by the profile of the Mo back contact, which, as interdiffusion between the Mo layer and the chalcopyrite is known to be negligible, should be a step function in the ideal case. Figure 3.23 (a) shows atomic ratios of $\frac{[Cu]}{[Cu]+[In]+[Ga]}$, $\frac{[S]}{[Cu]+[In]+[Ga]+[S]}$, and $\frac{[Ga]}{[In]+[Ga]}$, derived from SNMS depth profiles of a set of absorber layers with varied precursor $\frac{[Ga]}{[In]+[Ga]}$ ratio sulfurized at $T_{sulf} = 550^\circ \text{C}$, $t_{sulf} = 30 \text{ min}$. The atomic ratios of a set of samples sulfurized from identical precursors but sulfurized at varied temperatures are shown in

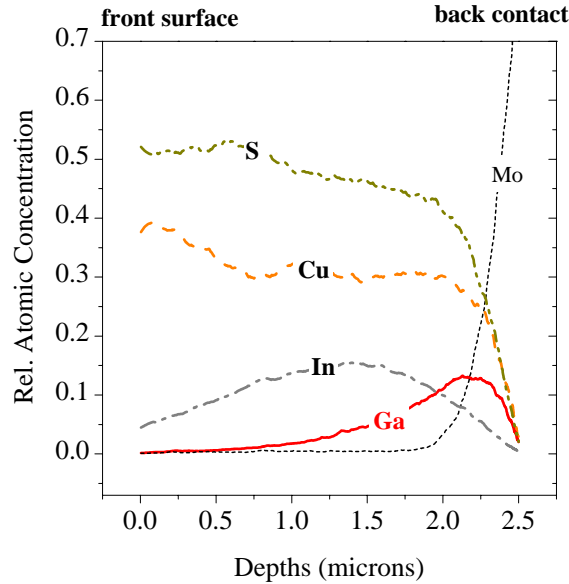


Figure 3.22: SNMS depth profile of a Ga-containing absorber layer.

Figure 3.23 (b). All samples show a distinct drop in Cu concentration near the surface, which is a typical feature for SNMS profiles of Cu-chalcopyrite, caused by sputter induced Cu migration [67]. There is a strong gradient in Ga concentration in all absorber films. There is an almost constant $[Ga]/([In] + [Ga])$ ratio near the surface, an intermediate region of increasing Ga concentration and a maximum close to the back contact. Increased sulfurization temperature causes a higher Ga concentration in the top region of the absorber close to the surface and a more extended intermediate region. As can be seen in Figure 3.23 (a) for a given sulfurization temperature higher $[Ga]/([In] + [Ga])$ ratios in the precursor also lead to an enhanced Ga concentration in the region near to the surface.

From the observed dependence of the Ga-depth profiles on the temperature during reactive annealing it can be concluded that the In-Ga intermixing process is governed by a diffusion process. In order to gain a rough estimate of the order of magnitude of the corresponding diffusion coefficient numerical fits have been applied to the measured depth profiles in the vicinity of the intermediate region between the $CuInS_2$ and the $CuGaS_2$ layers. These fits were based on an analytical solution to Fick's second law for the case of a pair of semi-infinite slabs (see e.g. [134]). The fits indicate interdiffusion coefficients for a $CuInS_2/CuGaS_2$ couple in the order of $10^{-12} \text{ cm}^2\text{s}^{-1}$ at $T = 550 \text{ }^\circ\text{C}$. This value is in reasonable agreement with results obtained for $CuInSe_2/CuGaSe_2$ thin film diffusion couples at slightly different processing temperatures derived on the basis of a similar simple model by Marudachalam [134]. However, it has to be noted that the applied model oversimplifies the physical situation and a more detailed discussion of the interdiffusion process taking into account the finite geometry and grain boundary effects will be given in Section 3.5.2.

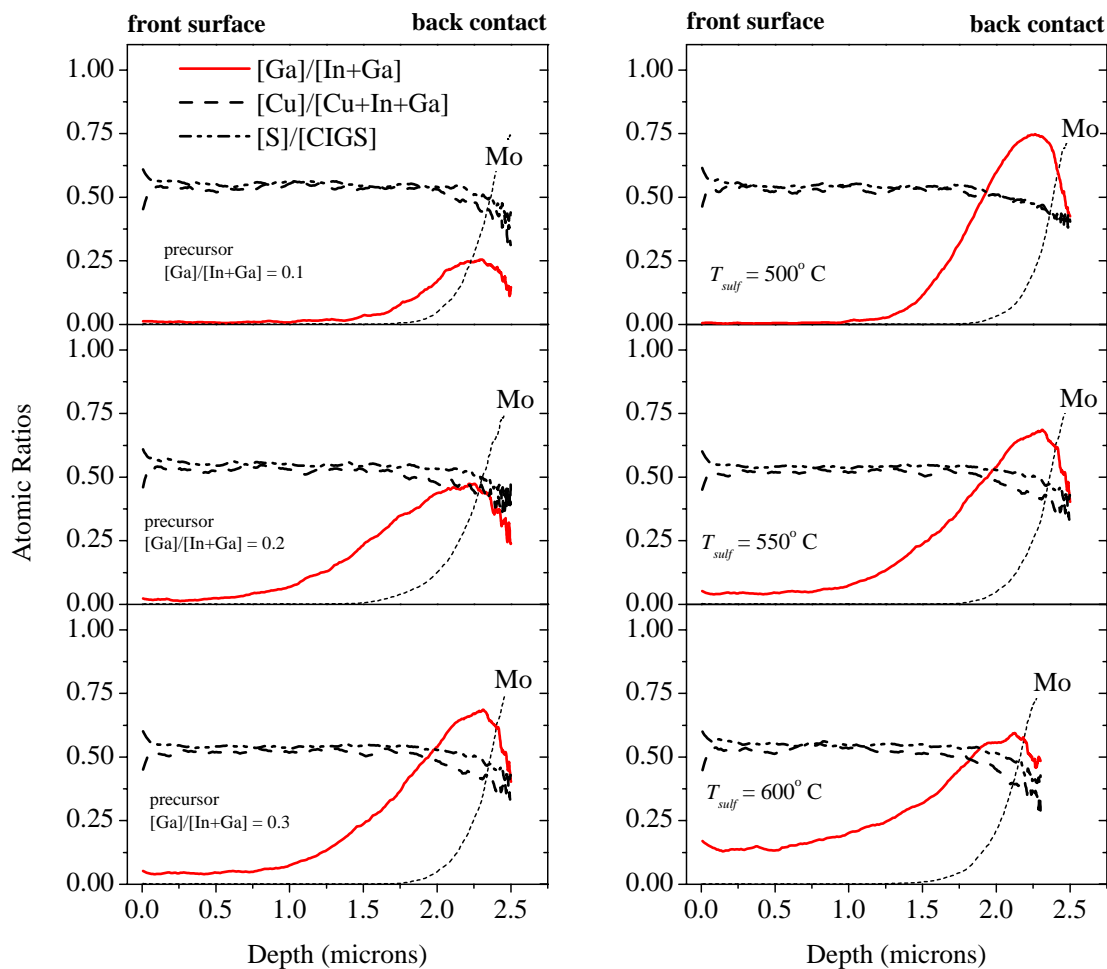


Figure 3.23: Depth profile of atomic ratios of $\text{Cu}(\text{In}_{1-x}\text{Ga}_x)\text{S}_2$ absorber films as determined by SNMS measurements. (a) Effect of varied precursor $[\text{Ga}]/([\text{In}] + [\text{Ga}])$ ratio, all samples were sulfurized in sulfur vapor at 550°C for 30 min. (b) Effect of sulfurization temperature T_{sulf} for samples processed from identical precursor ($[\text{Ga}]/([\text{In}] + [\text{Ga}]) = 0.3$) and sulfurized for 30 min.

Raman In Section 3.2.4 the two phase structure of the absorber was demonstrated by depth resolved micro-Raman spectroscopy. Figure 3.24 shows similar Raman spectra of the three Ga-containing samples sulfurized at 500 °C, 550 °C, and 600 °C of Figure 3.23 (b). The bottom spectra correspond to measurements at the samples surface, and spectra measured after each sputter step are vertically shifted.

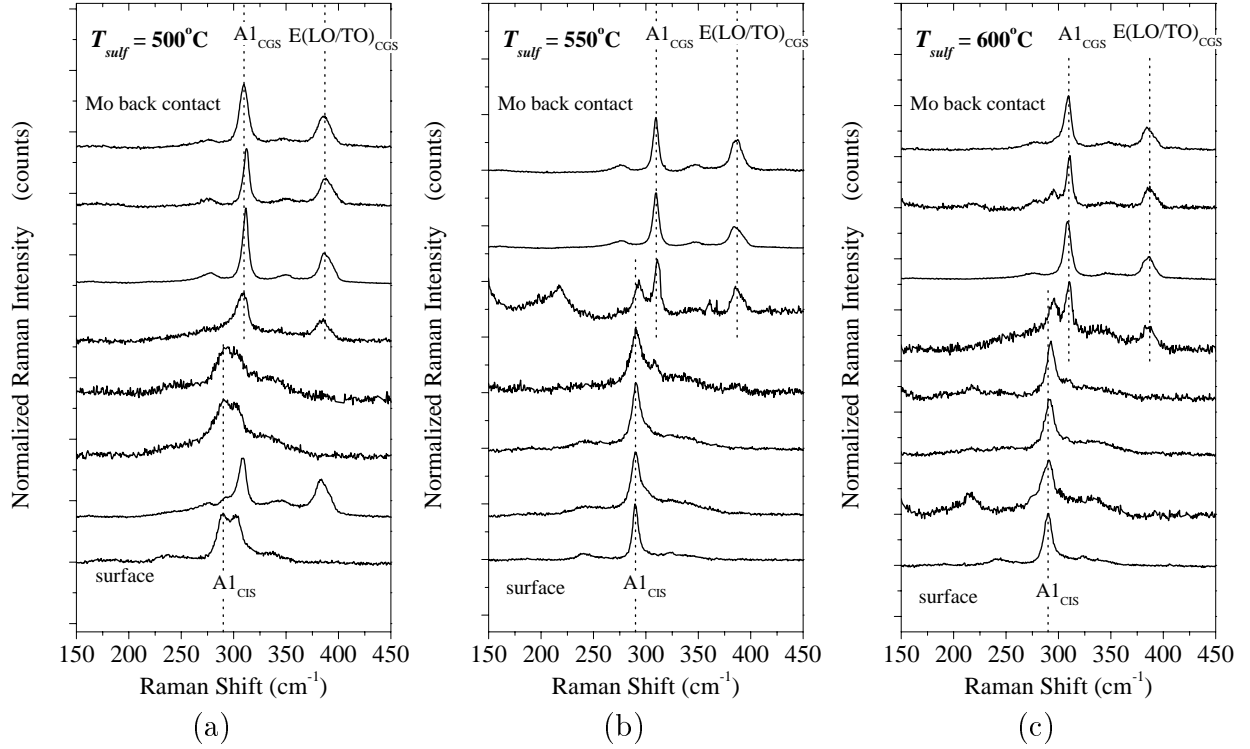


Figure 3.24: Normalized Raman spectra repeatedly taken between ion sputtering steps at $\text{Cu}(\text{In}_{1-x}\text{Ga}_x)\text{S}_2$ absorber layers (precursor $[\text{Ga}]/([\text{In}] + [\text{Ga}])$ ratio = 0.3) sulfurized in sulfur vapor at (a) $T_{\text{sulf}} = 500^\circ\text{C}$, (b) $T_{\text{sulf}} = 550^\circ\text{C}$, (c) $T_{\text{sulf}} = 600^\circ\text{C}$. The secondary copper sulfide phase had been etched off.

As was discussed in Section 2.2.1 the sputter rate of CuInS_2 differs from that of CuGaS_2 and as spectra were taken at equal time intervals they do not necessarily correspond to equidistant steps in thickness. All spectra are dominated by the A1-mode, which corresponds to the totally symmetric vibration of the anion-sublattice (Section 2.2.2). There is a clear transition from the CuInS_2 A1_{CIS} mode at 290 cm^{-1} to the CuGaS_2 A1_{CGS} mode at 310 cm^{-1} and there is only one spectra where both modes are present. Figure 3.25 plots the peak position and the full peak width at half maximum (FWHM) of the A1-mode versus increasing sputter time or samples depth, respectively. The dotted lines in the plots refer to data of CuInS_2 and CuGaS_2 single crystal measured with the same experimental set up. As can be seen the peak positions of the A1 mode of the CuInS_2 as well as the CuGaS_2 phase do not change significantly with depth which indicates a rather homogeneous composition in the top and in the back layer. In the case of the CuInS_2

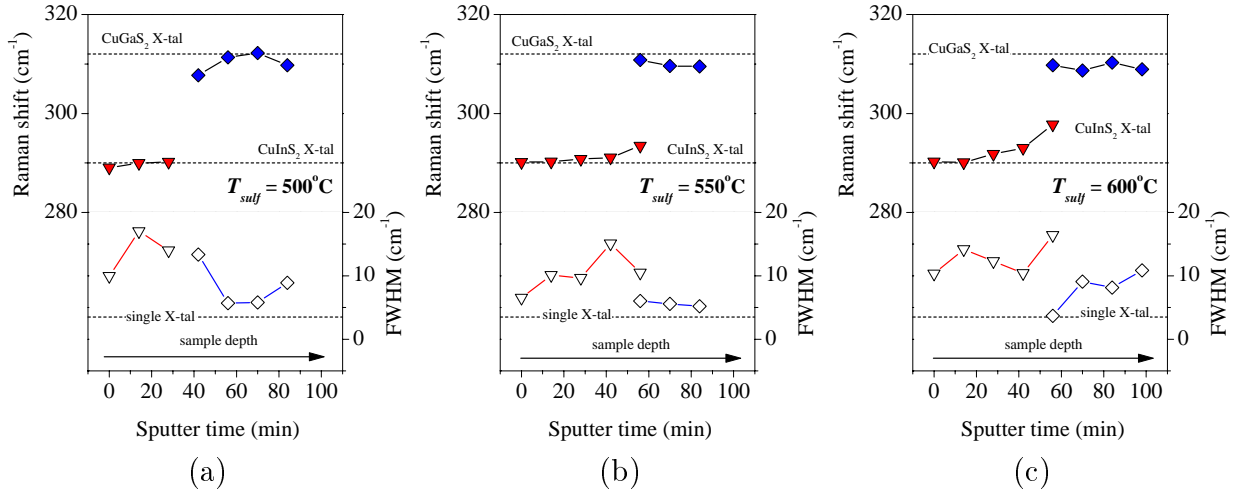


Figure 3.25: Position of the A1 Raman mode versus sputter time for samples sulfurized at (a) $T_{sulf} = 500^\circ\text{C}$, (b) $T_{sulf} = 550^\circ\text{C}$, (c) $T_{sulf} = 600^\circ\text{C}$. The corresponding Raman spectra are shown in Figure 3.24.

top phase this agrees with the constant Ga-concentrations found by SNMS for the near surface region. Only the sample sulfurized at 600°C shows a small but systematic shift in the A1-mode peak position of the top layer with increasing sample depth. No trend in peak position can be seen for the CuGaS₂ back phase, which would suggest that In - Ga intermixing mainly affects the top phase. It must be noted, however, that the evaluation of the Ga-content x of a Cu(In_{1-x}Ga_x)S₂ crystallite (Section 2.2.2) on the basis of the peak position of the A1-mode is not straight forward as the peak position does also depend on structural properties. According to Álvarez García et. al. [135] the A1 mode position of In-rich CuInS₂ films ($\Delta m < 0$) or films processed at low temperature is shifted to higher wave numbers with respect to the position known from reference single crystals. Since the shift is generally accompanied by a broadening of the mode it was assigned to a decrease in structural quality (higher density of lattice defects and/or smaller crystal domains) of the film under the respective preparation conditions. Figure 3.25 indicates that both effects, Ga alloying and changes in the structural quality, are present in the Cu(In_{1-x}Ga_x)S₂ absorber films. Nevertheless the general trend of enhanced In-Ga intermixing at higher sulfurization temperatures, as suggested by the SNMS depth profiles, is verified by the depth resolved Raman spectra of Figure 3.24. The values of the full width at half maximum (FWHM) of the observed A1-modes (Figure 3.25) reveal that peak broadening seems to be more pronounced near the CuInS₂/CuGaS₂ interface, which indicates a lower structural quality in this region. Since there is no systematic correlation to the sputter time sputter related damage of the crystal lattice, which would also lead to a broadened mode, can be ruled out. The most likely interpretation of the observed broadening behavior is the presence of a sphalerite phase of intermediate composition ($[\text{Ga}]/([\text{In}] + [\text{Ga}]) \approx 0.5$) at the CuInS₂/CuGaS₂ interface which, as discussed in Section 3.3 (Figure 3.17), can be observed during film growth.

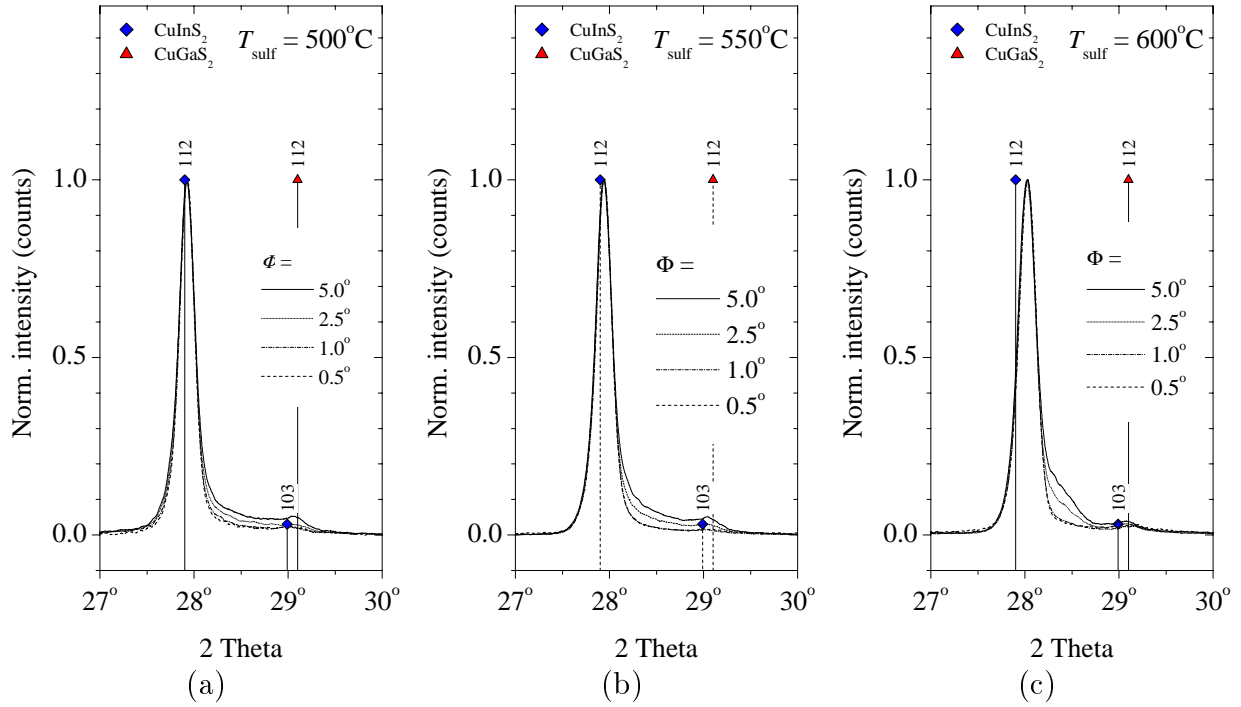


Figure 3.26: Normalized XRD spectra of $\text{Cu}(\text{In}_{1-x}\text{Ga}_x)\text{S}_2$ absorber layers (precursor $[\text{Ga}]/([\text{In}] + [\text{Ga}])$ ratio = 0.3) sulfurized in sulfur vapor at (a) $T_{\text{sulf}} = 500^\circ\text{C}$, (b) $T_{\text{sulf}} = 550^\circ\text{C}$, (c) $T_{\text{sulf}} = 600^\circ\text{C}$, measured in asymmetric mode at different angles of incidence Φ . The secondary copper sulfide phase had been etched off prior to the measurement.

XRD The existence of a phase of intermediate composition is also indicated by X-ray diffraction measurements. Asymmetric X-ray diffraction measurements which, as discussed in Section 2.2.3, allow for varying the sampling volume of a XRD measurement, verify the inhomogeneous Ga depth profile. Figure 3.26 shows the XRD spectra in the vicinity of the $(112)_{(\text{CuInS}_2)}$ reflex of the three samples already discussed in the previous paragraphs annealed at various sulfurization temperatures for 30 min. All spectra are normalized to the integrated peak intensity of the (112) reflection of the CuInS_2 top phase which dominates all spectra. The XRD spectra stay well above the baseline in between the $(112)_{(\text{CuInS}_2)}$ and the $(112)_{(\text{CuGaS}_2)}$ maxima which confirms the existence of a quaternary phase with varying $[\text{Ga}]/([\text{In}] + [\text{Ga}])$ ratio. The ambiguity caused by the overlap of the $(112)_{(\text{CuGaS}_2)}$ and the $(103)_{(\text{CuInS}_2)}$ reflections is resolved by evaluating the higher order CuGaS_2 reflections. The relative intensity of the reflections which are due to the CuGaS_2 layer and due to the intermediate layer decrease at lower angle of incidence, where the measurement is more surface sensitive, and eventually vanishes for incident angles below $\Phi = 1.0^\circ$, where 99 % of the incident X-ray radiation is absorbed in the first $1\ \mu\text{m}$ of the layer (see Figure 2.11). This agrees well with the thickness of the top region of almost constant Ga concentration as determined by SNMS. Furthermore the XRD measurements verify that the composition of the CuInS_2 top phase is homogeneous between the surface and a depth of $1\ \mu\text{m}$. With increasing sulfurization temperature and enhanced In-Ga intermixing the XRD-peaks

of the CuInS_2 top phase start to shift towards higher angles. An exact quantification of Ga alloying has been performed by determining the unit cell dimensions. The lattice constants a and c have been obtained by a simultaneous least-square fit of the peak positions of the six strongest XRD-reflections according to Equation (2.4). The resulting values are listed in Table 3.6. For low Ga-concentrations (acc. to SNMS) the lattice constants a and c are not significantly affected. In particular a dependence of the Ga-content of the top phase on the precursor Ga-content which was clearly observed by SNMS (Figure 3.23), is not reflected by a corresponding shift in lattice constant. A clear shift of a and c is only observed for samples with $[\text{Ga}]/([\text{In}] + [\text{Ga}]) > 0.1$. Figure 3.27 plots the lattice constant values for samples sulfurized at 550°C , ($[\text{Ga}]/([\text{In}] + [\text{Ga}]) < 0.1$) and 600°C ($[\text{Ga}]/([\text{In}] + [\text{Ga}]) > 0.1$). Also in the plot is a dotted line which corresponds to literature data of the $\text{Cu}(\text{In}_{1-x}\text{Ga}_x)\text{S}_2$ alloy system [25]. The discrepancy between the nominal Ga-content of samples with a $[\text{Ga}]/([\text{In}] + [\text{Ga}])$ ratio below 0.1 and the dotted line can clearly be seen. The error bars in the figure indicate that this is not due to experimental errors of the a and c values.

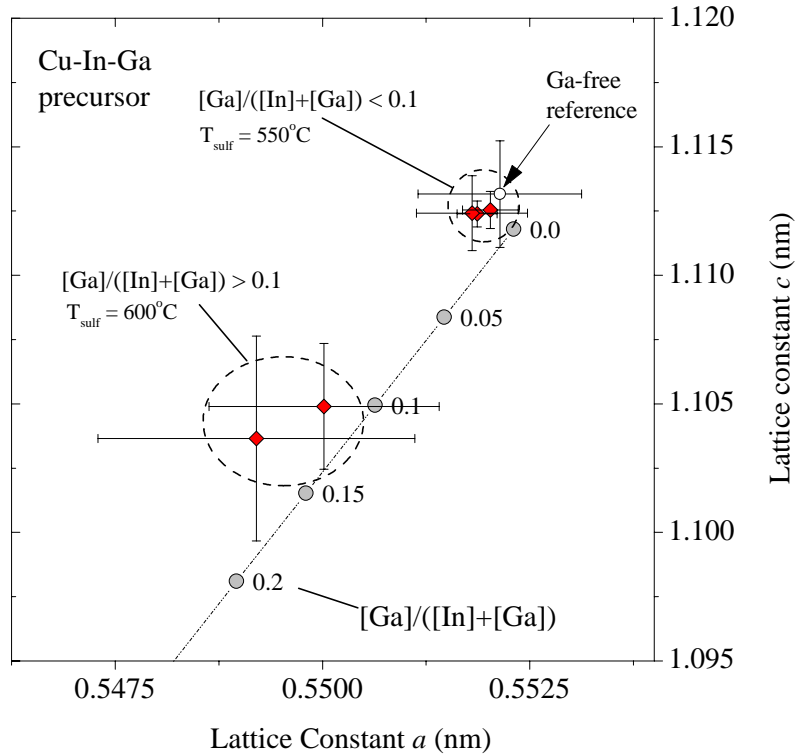


Figure 3.27: Experimental values of $\text{Cu}(\text{In}_{1-x}\text{Ga}_x)\text{S}_2$ solar cell absorber layers. Lattice constants have been determined by a least-square fit of the peak position of the six strongest reflections of the CuInS_2 top phase. The dotted line refers to values measured at single crystal $\text{Cu}(\text{In}_{1-x}\text{Ga}_x)\text{S}_2$ specimen [25]. The error bars indicate the confidence interval of the fitted lattice constants.

It has to be concluded that the incorporation does not purely act via In-Ga substitution at the group III atomic site of the chalcopyrite unit cell but that it involves other mechanisms

Table 3.6: Lattice constants of CuInS₂ absorber layers and top phase of Cu(In_{1-x}Ga_x)S₂ absorber layers processed from (I) Cu-In and (II)/(III) Cu-(In,Ga) precursors, respectively. Although the top phase of sample II contains Ga the lattice parameters are almost the same as in the Ga-free sample I.

sample	I	II	III
[Ga]/([In] + [Ga]) in precursor	0	≈ 0.3	≈ 0.3
sulfurization (in sulfur vapor)	550 °C, 30 min	550 °C, 30 min	600 °C, 30 min
[Ga]/([In] + [Ga]) in CuInS ₂ top phase (acc. to SNMS)	0	0.05	0.14
unit cell parameters			
<i>a</i>	0.5521 ± 0.001	0.5518 ± 0.001	0.549 ± 0.002
<i>c</i>	1.113 ± 0.002	1.112 ± 0.002	1.104 ± 0.003
<i>c/a</i>	2.016	2.016	2.009

such as:

(i) Ga occupation of vacant lattice sites or interstitial sites rather than the atom III site, or

(ii) Ga incorporation at grain boundaries only, thus the bulk concentration in the crystallites is significantly lower than the integral concentration.

Point (i) will be dealt with in Appendix A.1 whereas point (ii) will be discussed in the following.

3.5.2 CuGaS₂/CuInS₂ Diffusion Couples

In order to quantify the Ga-In intermixing process independently from the film growth process CuGaS₂/CuInS₂ diffusion couples have been prepared. These diffusion couples were meant to resemble a solar cell absorber layer shortly after the incorporation of sulfur has finished and before substantial intermixing of the cations sets in. In particular this approach allowed to separate the In-Ga interdiffusion process from the recrystallization process, since as was shown in the Section 3.5.2 both processes occur in parallel during film growth.

A layer of CuGaS₂ of 400 nm thickness was deposited onto an already processed 2 μm thick CuInS₂ layer. Both layers were deposited under Cu-excess. The secondary phase was removed after CuInS₂ deposition, but it was left at the sample surface after CuGaS₂ composition. The CuInS₂-CuGaS₂ stacking sequence, which is typical for absorber layer preparation, was reversed here to allow for better XRD-characterization of the thinner CuGaS₂ layer. The schematic structure and a SEM cross-section of such a CuInS₂/CuGaS₂

bilayer are depicted in Figure 3.28.

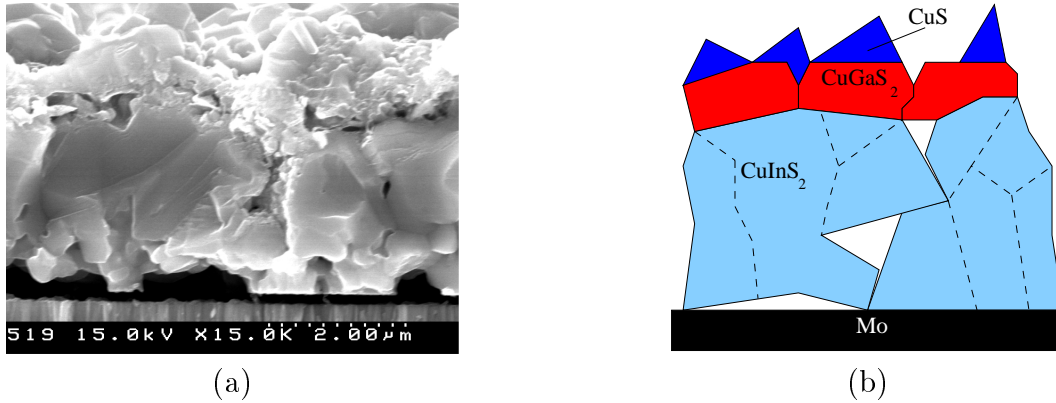


Figure 3.28: $\text{CuGaS}_2/\text{CuInS}_2$ diffusion couple (prepared as described in text). (a) SEM cross section, (b) schematic structure.

The bilayers were then annealed for 30 min at different temperatures. During annealing the layers were kept in an $\text{H}_2\text{S}/\text{Ar}$ atmosphere to avoid the sublimation of sulfur from the diffusion couple. The resulting loss of sulfur, which would be temperature dependent, would lead to additional sulfur vacancies in the chalcopyrite lattice. As a result new diffusion path ways would be created by the changed defect chemistry of the lattice. Enhanced In-Ga interdiffusion in a chalcogen free ambient has indeed been observed by Marudachalam [136] at $\text{CuInSe}_2/\text{CuGaSe}_2$ thin film diffusion couples.

The elemental depth distribution after annealing was measured by SNMS depth profiles, the phase composition was determined by XRD measurements.

Figure 3.29 shows the SNMS depth profiles of the unannealed diffusion couple plus three samples annealed at different temperatures for 30 min. As can be seen in the figure the $\text{CuInS}_2/\text{CuGaS}_2$ interface in the as deposited sample is not perfectly sharp which indicates a certain amount of In-Ga interdiffusion already during the CuGaS_2 layer deposition. Additional broadening is likely to be caused by the surface roughness of the diffusion couple. Considering the $[\text{Ga}]/([\text{In}] + [\text{Ga}])$ depth profile a similar intermixing behavior as during absorber layer growth is observed. There is a maximum in Ga concentration close to the surface, an intermediate region of varied Ga concentration and a region of almost constant concentration towards the back contact. With increasing annealing temperature the maximum Ga-concentration at the surface drops and the intermediate region extends further into the original CuInS_2 layer. At 550°C there is an almost constant $[\text{Ga}]/([\text{In}] + [\text{Ga}])$ gradient between the surface and the back of the bilayer.

From the XRD-spectra of the same set of samples, which are plotted in Figure 3.30, it can be seen that the two phase structure of the film is retained for all samples. With increasing annealing temperature the enhanced incorporation of Ga or In respectively is reflected by a shift of the (112) reflection of the CuInS_2 and the CuGaS_2 layer towards higher or lower angles, respectively. Hereby the shift of the $(112)_{\text{CuGaS}_2}$ is more pronounced. At 550°C the two reflections have almost merged into one peak.

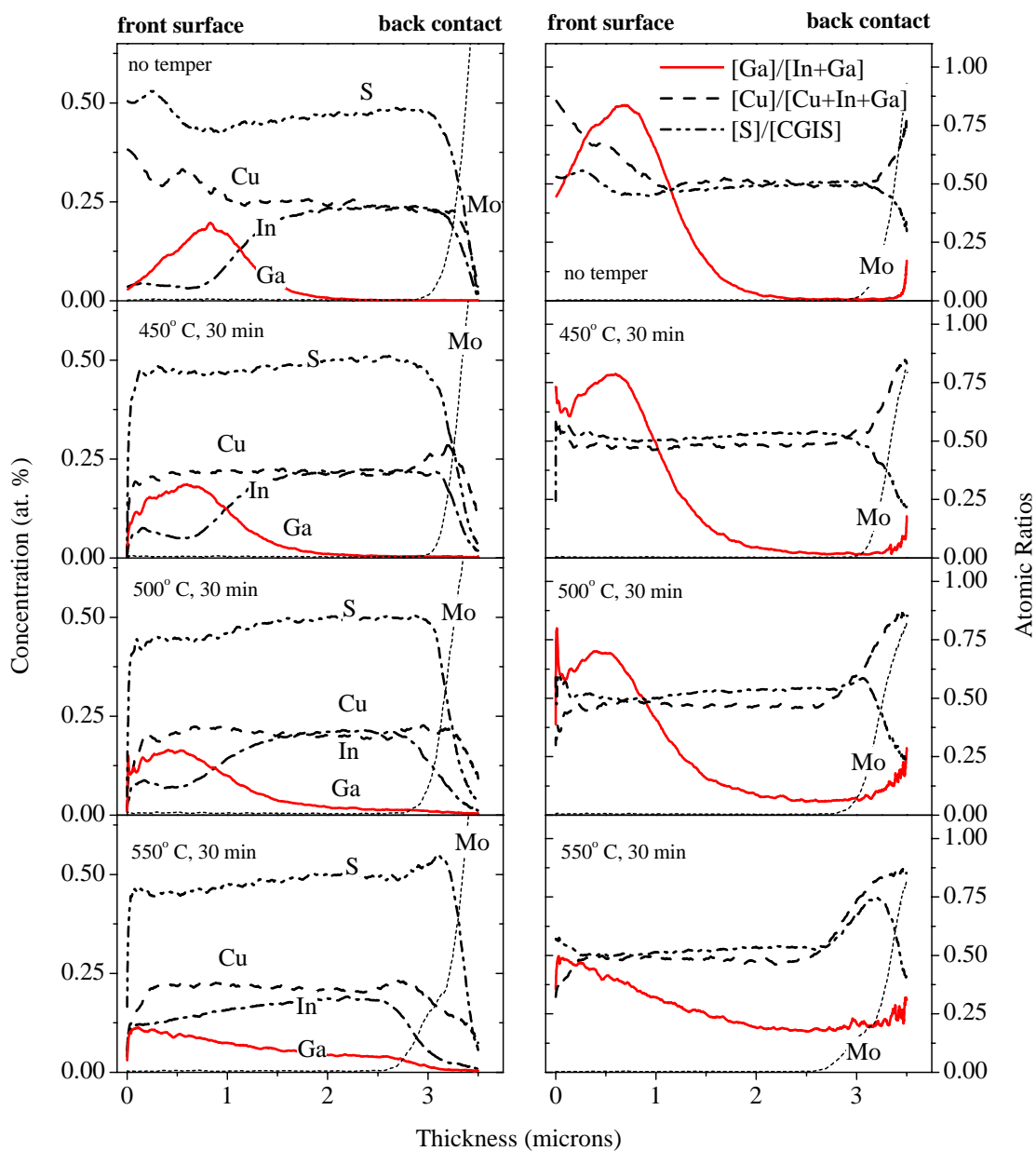


Figure 3.29: SNMS depth profile of $CuGaS_2/CuInS_2$ diffusion couples annealed in H_2S/Ar at different temperatures for 30 min: (a) atomic concentrations, (b) atomic ratios.

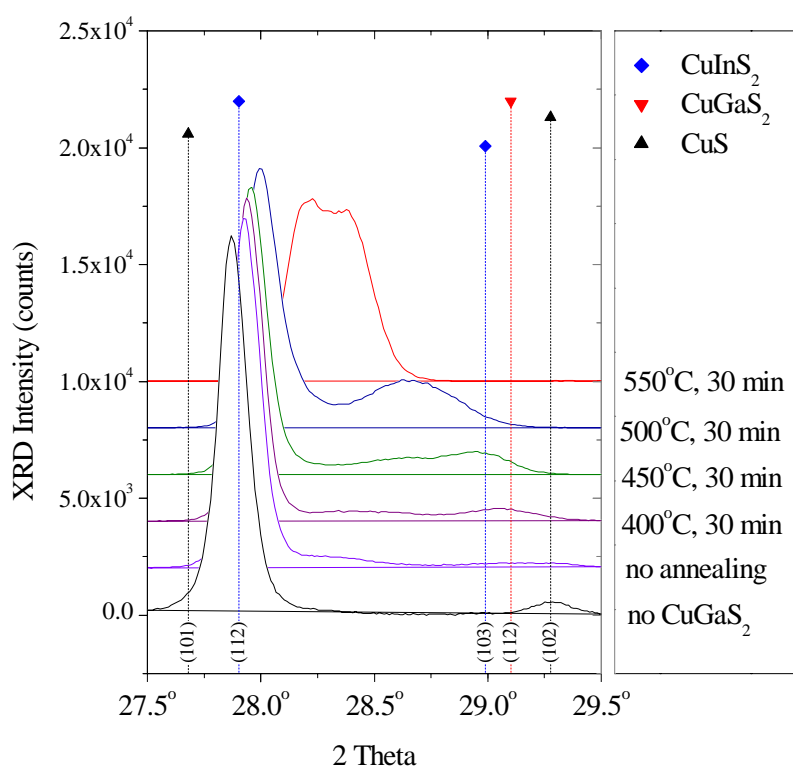


Figure 3.30: Dependence of (112) XRD reflections of $\text{CuGaS}_2/\text{CuInS}_2$ diffusion couple on annealing. Sample were annealed for 30 min in an $\text{H}_2\text{S}/\text{Ar}$ atmosphere. The two plots at the bottom refer to the CuInS_2 layer before CuGaS_2 deposition and the $\text{CuInS}_2/\text{CuGaS}_2$ couple before the annealing step.

All samples in Figure 3.30 had been annealed with the secondary copper-sulfide phase still at the sample surface. A comparison with samples where the copper-sulfide phase was removed before annealing shows that without the secondary phase at the sample surface In-Ga interdiffusion is less effective. Figure 3.31 shows XRD spectra of two such diffusion couples annealed at 550 °C for 30 min. The peak position of the (112)_{CuInS₂} reflection of the samples without copper sulfide has not changed at all indicating that most of the CuInS₂ layer was not affected by the interdiffusion process.

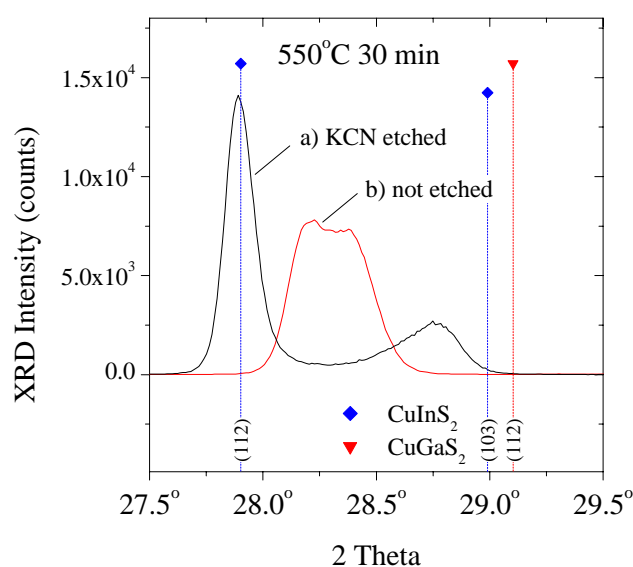


Figure 3.31: (112) reflections of CuGaS₂/CuInS₂ diffusion couples annealed in H₂S/Ar at 550 °C for 30 min: (a) secondary copper sulfide phase removed before annealing, (b) annealed with copper sulfide present in the sample.

When comparing the experimental results obtained by SNMS, Raman and XRD with respect to the In-Ga intermixing during film growth or at the diffusion couples the following characteristics can be deduced.

- (i) despite the interdiffusion of Ga and In the bilayer mainly retains its two phase structure of two layers of almost homogeneous composition,
- (ii) the composition of these layers depends on the processing temperature, i.e. increasing sulfurization temperature leads to enhanced interdiffusion.
- (iii) the interdiffusion process is much more effective if copper sulfide is present in the sample.

In the following section an inter diffusion model will be introduced which allows to deduce the diffusion coefficients for In-Ga interdiffusion on grounds of the presented experimental results.

3.5.3 Interdiffusion Model

The In-Ga interdiffusion process has been analyzed quantitatively by modeling the Ga-depth profile according to an analytical model. XRD spectra have been calculated on the basis of the assumed Ga-depth profile (see Section 2.2.4). The simulated XRD spectra have been fitted to the measured XRD spectra by varying the Ga-depth profile. The sputter profiles served as an unambiguous starting point for the fitting procedure. Whereas the depth resolution of the sputtering experiments is limited due to the rough morphology of the absorber film the non-destructive nature of the XRD measurement provides valuable complimentary information about the depth profile. By means of the XRD simulations the Ga-depth profiles could be evaluated with high depth resolution in a non-destructive way.

In the following the diffusion process will be described in terms of the Ga-depth profile. Lets assume that the In-Ga diffusion process is governed by Fick's second laws of diffusion, i.e.

$$\frac{\partial c}{\partial t} = D \frac{\partial^2 c}{\partial x^2}, \quad (3.8)$$

where c is the concentration of the diffusion species, and D is the diffusion coefficient. All diffusion coefficients may be isotropic and independent of concentration, position and time. There is no net flow of material out of the sample, i.e. the front surface $x = 0$ and the back surface $x = l$ of the thin film act as reflecting boundaries, i.e.

$$\left. \frac{\partial N(x, t)}{\partial x} \right|_{x=0} = \left. \frac{\partial N(x, t)}{\partial x} \right|_{x=l} = 0. \quad (3.9)$$

At the beginning of the diffusion process ($t = 0$) the Ga-depth profile is described by a step function, which refers to the initial situation of the diffusion couples as well as to the clear phase separation of CuInS₂ and CuGaS₂ found during film growth. Thus

$$c(x, 0) = \begin{cases} 1; & x \leq h \\ 0; & x > h \end{cases}. \quad (3.10)$$

Here h corresponds to the thickness of the CuGaS₂ layer and l to the thickness of the entire CuGaS₂/CuInS₂ layer. Using these boundary and initial conditions an analytical solution based on a general solution of Fick's second law [137] has been derived. The Ga concentration $c(x, t)$ is then given by

$$c(x, t) = \left(\frac{2}{l} \sum_{m=0}^{\infty} e^{-(\frac{m\pi}{l})^2 Dt} \cos\left(\frac{m\pi}{l}x\right) \frac{l}{\pi m} \sin\left(\frac{m\pi}{l}h\right) \right) + \frac{h}{l}. \quad (3.11)$$

A series of numerical evaluations of Equation (3.11) for a diffusion couple of a 0.5 μm CuGaS₂ layer and a 2.5 μm CuInS₂ layer is plotted in Figure 3.32 (a). Figure 3.32 (b) shows the corresponding XRD-spectra together with an experimental data set taken from

Figure 3.30. The calculated XRD spectra are in poor agreement with the experimentally observed spectra. Thus, it becomes evident that the Ga-depth profiles of the diffusion couples can not be described by a one-dimensional solution, In particular it becomes clear that the almost constant Ga concentration in the two bilayers of the absorber film does not result from the finite geometry of the sample, i.e. it is not due to accumulation of Ga at the reflecting boundaries.

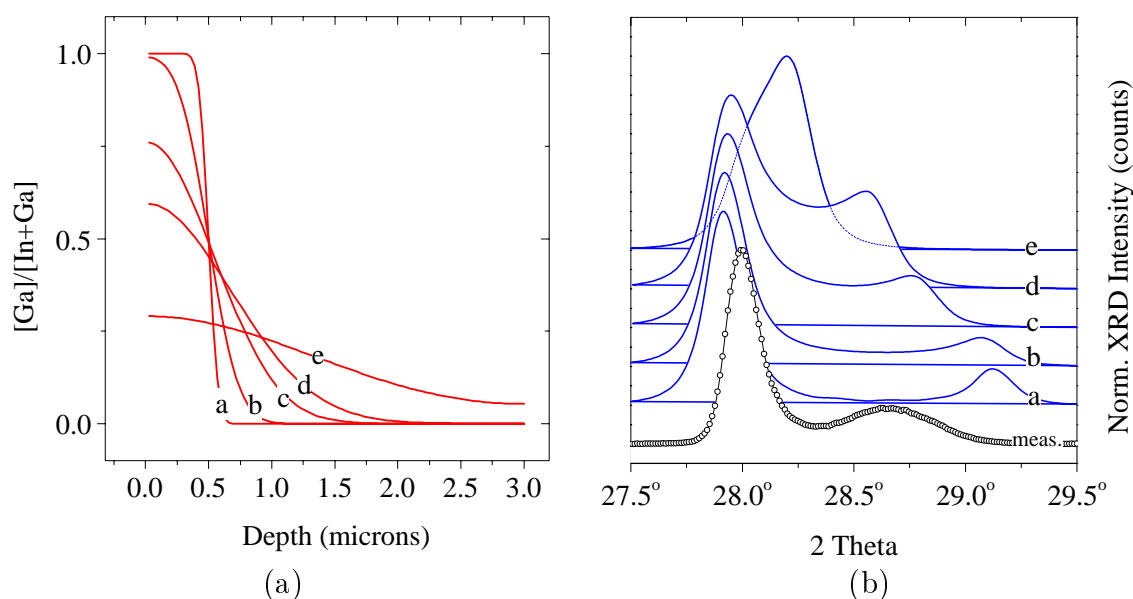


Figure 3.32: (a) Calculated Ga depth profile for one-dimensional diffusion between a $CuGaS_2$ layer (thickness $0.5\mu m$) and a $CuInS_2$ layer (thickness $2.5\mu m$). (b) Calculated (112) XRD reflection according to the Ga-depth profile of subfigure (a). All plots are normalized to the (112) $CuInS_2$ reflection. An experimental curve is plotted for comparison (lower most curve).

Therefore a two-dimensional model which accounts for the polycrystalline nature of the sample has been employed in order to simulate the Ga-depth profile. The general behavior of diffusion in polycrystals is given in Appendix A.2. Here In and Ga atoms are assumed to diffuse into the crystal grains via volume diffusion and also along grain boundaries. The term grain boundary shall refer to all kinds of paths of high atomic diffusivity such as interfacial regions between two grains of the same as well as two different phases and diffusion path ways along surface defects. In particular it shall also include diffusion via the secondary copper sulfide phase. The analytical treatment does not rely on a particular diffusion mechanism. All mechanism are rather lumped into two effects, which can be described by a net bulk and a grain boundary diffusion coefficient. The $CuInS_2$ and the $CuGaS_2$ layer are assumed to consist of columnar grains separated by grain boundaries perpendicular to the interface (Figure 3.33). The diffusion process of Ga into the $CuInS_2$ layer and In into the $CuGaS_2$ layer are calculated separately. In each case the other phase is considered to be a constant source of diffusant, which allows for the direct application of an

analytical solution of the diffusion equation given by Gilmer and Farrell [138]. The layered structure of the samples with an relatively sharp interface between the two phases which remained for all annealing conditions investigated justifies the assumption of a constant source. Nevertheless it has to be noted, that it is certainly an oversimplification of the experimental situation, since the layers are of finite thickness and the diffusant will deplete with ongoing diffusion.

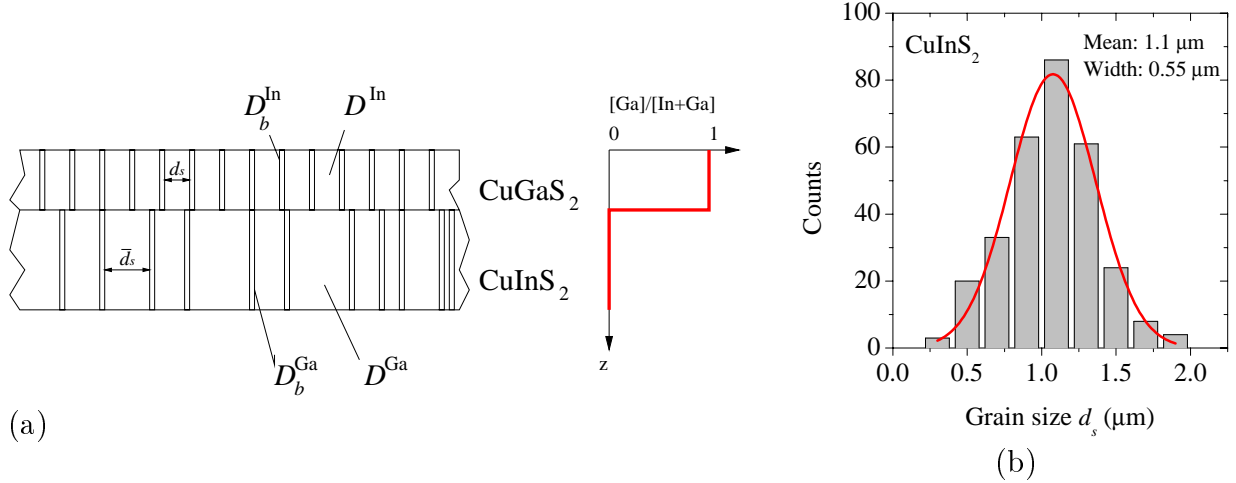


Figure 3.33: (a) Geometry of CuInS₂/CuGaS₂ diffusion couple and initial Ga-distribution at $t = 0$. Both layers are assumed to contain parallel grain boundaries of width d_s . (b) Grain size distribution of CuInS₂ layer [10].

Gilmer and Farrell [138] have studied diffusion from a constant source into a specimen of finite dimensions in the diffusion direction with uniformly spaced parallel grain boundaries. Their analytical solution is restricted to a type B kinetics regime, i.e. the diffusant fluxes from the neighboring boundaries do not interact (see Section A.2). The application of the solution to the current problem is justified by the condition for type B kinetics in a polycrystalline material given by Kaur [139]:

$$10\delta < (Dt)^{1/2} < d/10. \quad (3.12)$$

Equation (3.12) is graphically illustrated in Figure 3.34 for the case of a sample of $d = 1 \mu\text{m}$. Using the rough value of $10^{-12} \text{ cm}^2\text{s}^{-1}$ for Ga interdiffusion deduced from the SNMS sputter profiles of Figure 3.23 and an anneal time of $t = 30 \text{ min}$ it becomes clear from the figure that grain boundary diffusion in CuInS₂/CuGaS₂ diffusion couples in the observed temperature range are described by type B kinetics. Details on the analytical solution of Gilmer and Farrell can be found in Section A.2.1.

Figure 3.35 compares the experimental spectra of Figure 3.30 to calculated XRD spectra based on simulated Ga-depth profiles from the 2-dim grain boundary model. As can be seen the average concentration profile consists of two parts: a high-concentration steep part close

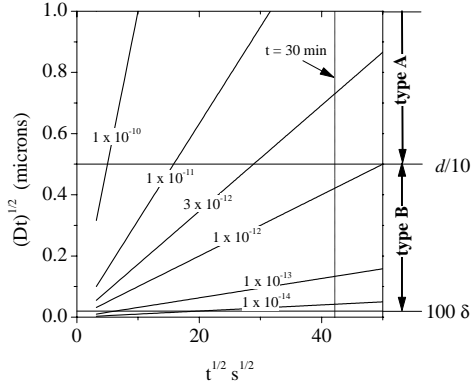


Figure 3.34: Depth of penetration $(Dt)^{1/2}$ of a diffusant as a function of time for different bulk diffusion coefficients. The vertical lines indicate the transition between type B and type A kinetics assuming a grain size of $1 \mu\text{m}$ and a grain boundary width of 2 nm .

to the $\text{CuInS}_2/\text{CuGaS}_2$ interface which is due to volume diffusion and a low-concentration flat part in the deeper region which represents grain boundary diffusion, Ga diffusion into the CuInS_2 layer was modeled using the grain size distribution of the CuInS_2 layer shown in Figure 3.33 (b), which was determined from a cross-sectional TEM image [10]. The Ga-depth distribution was calculated for nine grain size values d_s and the resulting XRD-spectra were then summed up according to the specific weight of the respective d_s value. Unfortunately no grain size data was available for the CuGaS_2 layer, so a d_s value of $0.2 \mu\text{m}$ (= half of the thickness of CuGaS_2 layer) was chosen. The final XRD spectra were obtained by varying the volume and grain boundary diffusion coefficients thereby varying the Ga-depth profile until agreement between XRD simulation and experimental data had been reached. In the case of the CuGaS_2 layer optimal agreement between measurement and simulation required an increase of the mean grain size of the CuGaS_2 film with increasing annealing temperatures, possibly due to an incomplete recrystallization of the CuGaS_2 layer during deposition. The determined diffusion coefficients are listed in Table 3.7.

Table 3.7: Chemical diffusion coefficients for thin film interdiffusion of In in CuGaS_2 and Ga in CuInS_2

T_{anneal} $^{\circ}\text{C}$	Ga \rightarrow CuInS_2			In \rightarrow CuGaS_2		
	D cm^2s^{-1}	δD_b cm^3s^{-1}	\bar{d}_s μm	D cm^2s^{-1}	δD_b cm^3s^{-1}	d_s μm
450	2×10^{-14}	3.8×10^{-19}	1.1	1×10^{-14}	7.5×10^{-19}	0.2
500	5×10^{-14}	1×10^{-17}	1.1	2×10^{-14}	1×10^{-17}	0.3
550	9×10^{-14}	1.2×10^{-16}	1.1	9×10^{-14}	1.2×10^{-16}	0.4

The simulated Ga-depth profiles in Figure 3.35 confirm that the relatively sharp interface between the CuInS_2 and the CuGaS_2 phase is retained in all samples. A fact which is also responsible for the clear transition between the CuInS_2 -A1 mode and the CuGaS_2 -A1 mode observed with Raman spectroscopy at Ga-containing absorber layers (Figure 3.24). According to Table 3.7 the values for the bulk diffusion coefficients do not differ much between In and Ga. Below 550°C the coefficients of Ga are slightly higher than the In values. Cation volume diffusion is known to act via vacancy in the lattice. The defect

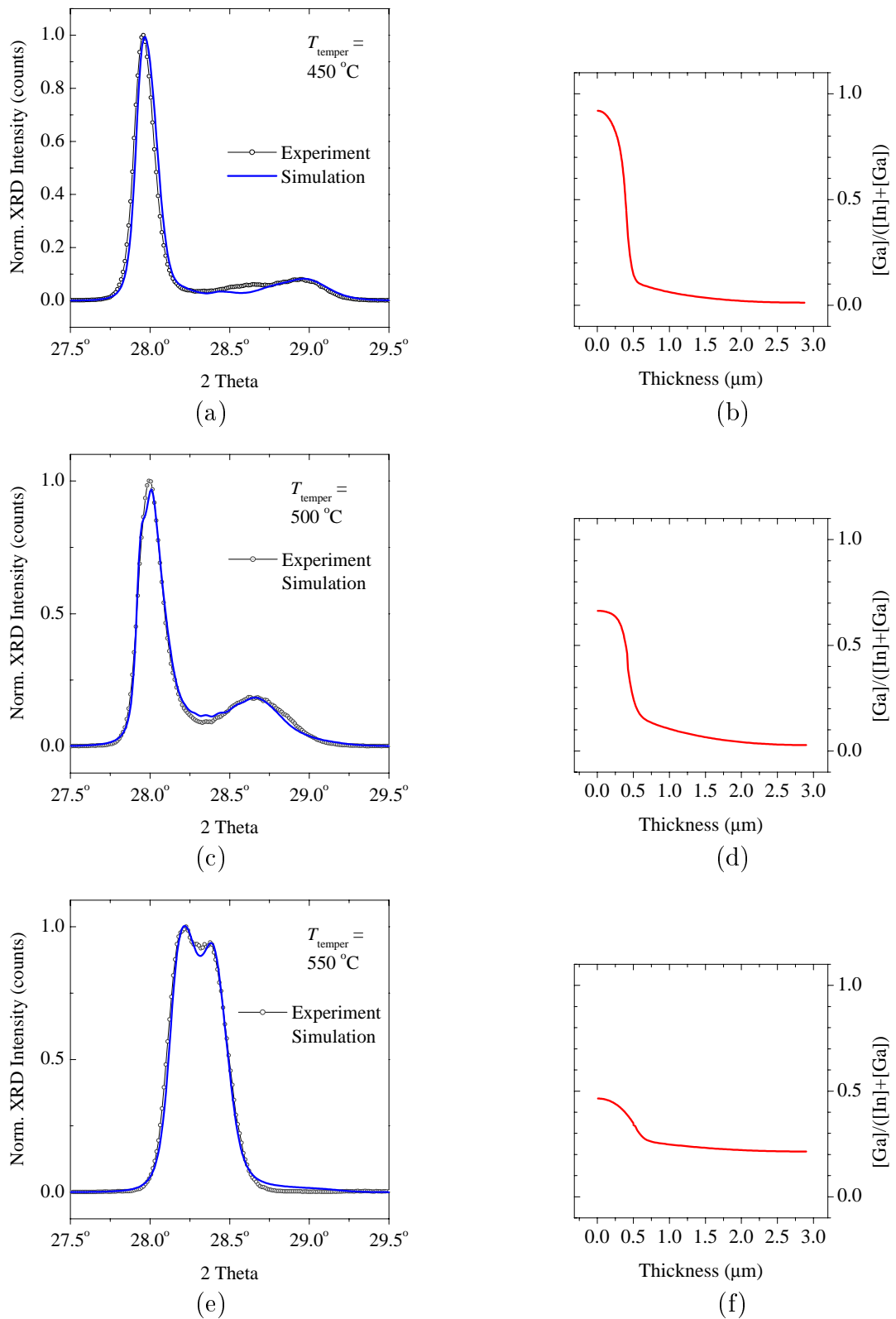


Figure 3.35: Calculated XRD spectra of $\text{CuGaS}_2/\text{CuInS}_2$ diffusion couples annealed for 30 min in a $\text{H}_2\text{S}/\text{Ar}$ atmosphere at different temperatures. The Ga-profiles were calculated using the parameters listed in Table 3.7.

complex of two Cu vacancies and one substitutional In at a Cu-site ($2V_{\text{Cu}} + \text{In}_{\text{Cu}}$) has been discussed by several authors as diffusion paths for cations in Cu-chalcopyrites [121, 136]. According to Zunger [124] the ($2V_{\text{Cu}} + \text{In}_{\text{Cu}}$) defect complex has a very low or, under certain conditions, even negative formation energy in the CuInSe_2 and in the CuGaSe_2 chalcopyrite lattice. Furthermore the formation energy is in general lower in the CuInSe_2 lattice than in the CuGaSe_2 lattice. Assuming a similar defect chemistry in the CuInS_2 - CuGaS_2 lattice a lower defect formation energy in CuInS_2 will offer a greater number of possible diffusion paths at a given temperatures and might explain the higher diffusivities of Ga in CuInS_2 with respect to In in CuGaS_2 . In most cases an Arrhenius equation

$$D = D_0 \exp(-Q/kT) \quad (3.13)$$

well describes the temperature dependence of the diffusion coefficient within the range of study [140]. D_0 is a pre-exponential factor and Q is the activation energy. Activation energies for the volume diffusion coefficients are in the range of 100 kJ/mol (see Figure 3.36 (b)). The crucial role of the copper-sulfide phase onto the recrystallization process was already discussed in Section 3.3. In terms of the tentative recrystallization model introduced in Section 3.3.3 the copper-sulfide was discussed as a channel of high-mobility for cations. In a similar way, there is a clear correlation between the In-Ga interdiffusion process and the presence of a copper sulfide binary phase (Figure 3.31), an effect which is in agreement with earlier reports on enhanced $\text{CuInSe}_2/\text{CuGaSe}_2$ alloying under the presence of copper chalcogenide phases [115]. Thus, from the results of this work it has to be concluded that channels of high-diffusivity, described by the δD_b coefficient in the diffusion model, are realized by diffusion via the secondary copper sulfide phase.

Figure 3.36 compares the deduced values of this work to chemical diffusion coefficients reported in literature for Ga and In in CuInSe_2 polycrystalline films [95] and epitaxial layers [141]. The values for In-diffusion in CuGaSe_2 , measured by Marudachalam [95], represent the only data found in literature describing the same temperature range as this work. All values of Marudachalam lie above the data of this work. The discrepancy between the two sets of data is mainly due to the fact that in this work effects of volume and grain boundary diffusion have been distinguished whereas in Marudachalam's analysis both effects go into one effective value for the diffusion coefficient. As a consequence the values derived in this work are smaller.

In conclusion, it could be shown that Ga and In intermixing during the reactive annealing step of Cu-(In,Ga) precursors is governed by diffusion. An analysis at $\text{CuInS}_2/\text{CuGaS}_2$ thin film diffusion couples revealed that in the observed range of temperatures (which corresponds to typical growth temperatures of chalcopyrite thin film growth on glass substrates) the diffusional transport process can well be described by thin film grain boundary diffusion. The secondary copper sulfide phase could be identified as the high diffusivity pathway involved in the diffusion process.

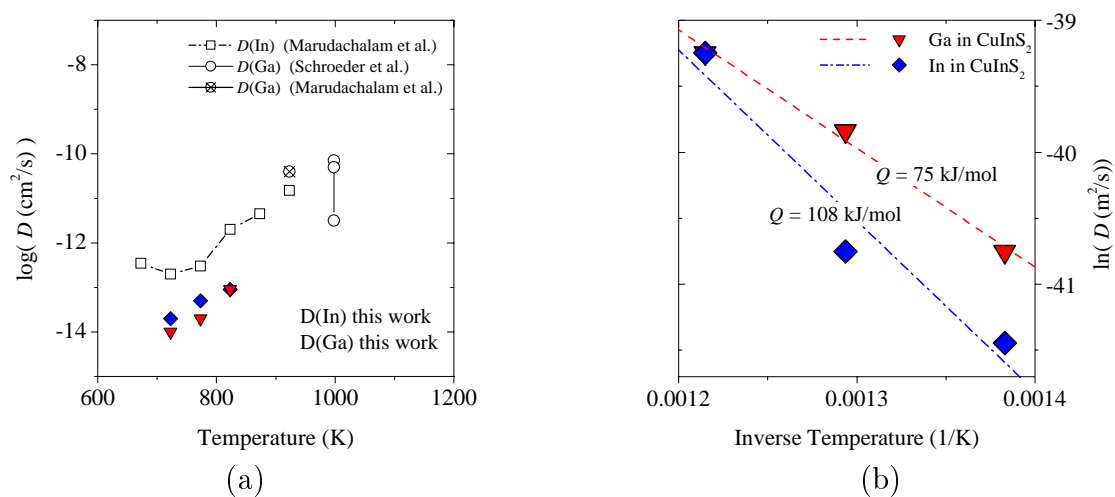


Figure 3.36: (a) Chemical diffusion coefficients of Ga in CuInX_2 and In in CuGaX_2 . open symbols: X=Se (taken from literature [95, 141]), filled symbols: X=S, this work. (b) Arrhenius plot of diffusion coefficients determined in this work.